HHS Public Access

Author manuscript

Mol Cell. Author manuscript; available in PMC 2019 February 01.

Published in final edited form as:

Mol Cell. 2018 February 01; 69(3): 371–384.e6. doi:10.1016/j.molcel.2018.01.012.

SLFN11 blocks stressed replication forks independently of ATR

Junko Murai[1,*], **Sai-Wen Tang**[1,†], **Elisabetta Leo**[1,‡], **Simone A Baechler**[1], **Christophe E. Redon**[1], **Hongliang Zhang**[1], **Muthana Al Abo**[1], **Vinodh N Rajapakse**[1], **Eijiro Nakamura**[2], **Lisa M. Miller Jenkins**[3], **Mirit I Aladjem**[1], and **Yves Pommier**[1,*,§]

[1]Developmental Therapeutics Branch and Laboratory of Molecular Pharmacology, Center for Cancer Research, National Cancer Institute, NIH, Bethesda, MD 20892, USA

[2]DSK project, Medical Innovation Center, Kyoto University Graduate School of Medicine, Kyoto, 606-8397, Japan

[3]Laboratory of Cell Biology, Center for Cancer Research, National Cancer Institute, NIH, Bethesda, MD 20892, USA

SUMMARY

SLFN11 sensitizes cancer cells to a broad range of DNA-targeted therapies. Here we show that, in response to replication stress induced by camptothecin, SLFN11 tightly binds chromatin at stressed replication foci via RPA1 together with the replication helicase subunit MCM3. Unlike ATR, SLFN11 neither interferes with the loading of CDC45 and PCNA nor inhibits the initiation of DNA replication but selectively blocks fork progression while inducing chromatin opening across replication initiation sites. The ATPase domain of SLFN11 is required for chromatin opening, replication block and cell death but not for the tight binding of SLFN11 to chromatin. Replication stress by the CHK1 inhibitor Prexasertib also recruits SLFN11 to nascent replicating DNA together with CDC45 and PCNA. We conclude that SLFN11 is recruited to stressed

[*]Correspondence: pommier@nih.gov; junko.murai@nih.gov.
[†]Current address: Division of Blood and Marrow Transplantation, Department of Medicine, Stanford University School of Medicine, Stanford, CA, USA
[‡]Current address: DNA Damage Response Biology, Oncology IMED, AstraZeneca, Hodgkin Building, B900 Chesterford Research Park, Little Chesterford, Cambridge CB10 1XL, U.K
[§]Lead Contact

DECLARATION OF INTEREST

The authors declare no competing interests.

SUPPLEMENTAL INFORMATION

Supplemental information includes seven figures and four tables, and can be found with this article online.

AUTHOR CONTRIBUTIONS

Y.P. supervised the study. J.M., Y.P. and E.L. devised the concept. Y.P., J.M., S.T., E.L., C.R., M.I.A., H.Z. and S.A.B. designed the experiments. J.M. generated and characterized *SLFN11*-deleted cell lines. S.T. generated and characterized *SLFN11*-overexpressing cell lines. J.M. and M.A.A. performed viability assays and analyzed the data. J.M. performed confocal microscopy analysis, DNA fiber assay, Western blotting, cell cycle analysis, iPOND, ChIP assay and analyzed the data. S.A.B. performed immunoprecipitation assay. S.A.B and L.M.M.J. performed the IP-MS and analyzed data. V.N.R. analyzed the *SLFN11* expression data. C.R. performed nascent strand DNA-seq, and C.R., M.I.A. and J.M. analyzed data. H.Z. performed ATAC-seq, and H.Z. and J.M. analyzed data. E.N. contributed with discussion and supported materials. J.M., Y.P. and S.T. wrote the manuscript.

replication forks carrying extended RPA filaments where it blocks replication by changing chromatin structure across replication sites.

eTOC Blurb

SLFN11 is a dominant determinant of sensitivity to DNA-targeted therapies. Murai et al. show that SLFN11 is recruited to stressed replication forks, open chromatin and block replication when replication is perturbed by DNA damage or improperly activated by cell cycle checkpoint inhibition. SLFN11 emerges as a unique S-phase regulator.

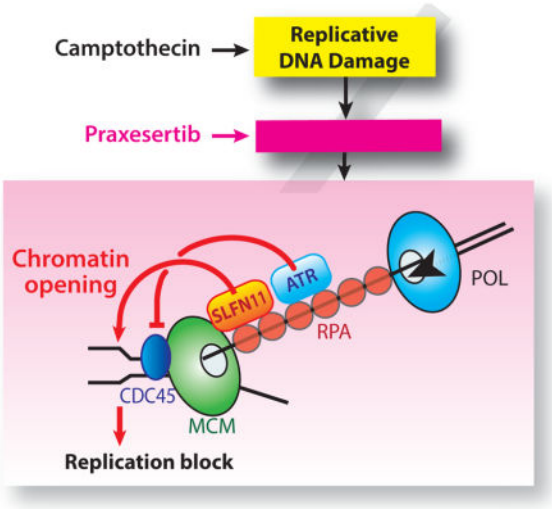

INTRODUCTION

The family of *Schlafen* (*SLFN*; "to sleep" in German) genes is only found in mammals (Mavrommatis et al., 2013). Among the *SLFN* genes, *SLFN11* was discovered by bioinformatics analyses of cancer cell databases as a dominant determinant of response to widely used anti-cancer drugs including topoisomerase I (TOP1) inhibitors [camptothecin (CPT), topotecan and irinotecan], topoisomerase II (TOP2) inhibitors (etoposide, mitoxantrone and doxorubicin), alkylating agents (cisplatin and carboplatin) and DNA synthesis inhibitors (gemcitabine and cytarabine) (Barretina et al., 2012; Nogales et al., 2016; Zoppoli et al., 2012). Moreover, a link between high SLFN11 expression and hypersensitivity to poly(ADP-ribose) polymerase (PARP) inhibitors has recently been established (Lok et al., 2017; Murai et al., 2016; Stewart et al., 2017). A common mechanism of action among these drugs is DNA damage leading to replication fork stalling with cell cycle checkpoint activation, also referred to as replication stress. CPT damages DNA by trapping TOP1 cleavage complexes (Pommier, 2006) and PARP inhibitors damage DNA by trapping PARP1/2-DNA complexes (Murai et al., 2012). Therefore, replication stress appears as the common mechanism(s) engaging SLFN11 to kill cancer cells.

In response to replication stress, the S-phase checkpoint acts as a central pathway coordinating DNA repair with replisome activity and origin firing to ensure genome integrity (Zeman and Cimprich, 2014). ATR (ataxia telangiectasia and Rad3-related) is a critical S-

phase checkpoint protein kinase. Its activation induces a global shutdown of origin firing throughout the genome and slows fork speed. ATR is activated by single-strand DNA (ssDNA) coated with replication protein A (RPA) at stalled replication forks and DNA-end resection sites (Branzei and Foiani, 2008). In turn, ATR activates checkpoint kinase 1 (CHK1) by phosphorylating its serine 345, which consequently inactivates cyclin-dependent and Dbf4-dependent kinases (CDK/DDK) that play pivotal roles for replication initiation. CDK/DDK promotes the loading of replication factors (CDC45, GINS, and others) onto replication origins (Fragkos et al., 2015) to activate the replicative helicase MCM2-7. Helicase activation induces the recruitment of replication factor C, proliferating cell nuclear antigen (PCNA) and the RPA complex consisting of RPA1, RPA2 and RPA3. Phosphorylation of CHK1 by ATR prevents unscheduled origin firing (Feijoo et al., 2001). Hence, ATR inhibitors (VE-821, AZD6738) and the CHK1 inhibitor LY2606368 (Prexasertib) induce unscheduled origin firing with excessive RPA loading at the ssDNA gaps generated by uncoupling between DNA polymerases and the MCM helicase. Consequently, ATR/CHK1 inhibitors leads to early mitosis where cells die by replication catastrophe (King et al., 2015; Syljuasen et al., 2005). This is the reason why ATR and CHK1 inhibitors alone or in combination with DNA damaging agents are being developed clinically to kill cancer cells harboring replicative stress.

SLFN11 is inactivated at the transcription level in approximately half of the cell lines across the available cancer cell line databases including the NCI-60 (Nogales et al., 2016), the CCLE (Barretina et al., 2012), and the Genomics of Drug Sensitivity in Cancer project (GDSC) (Yang et al., 2013) (Figure S1A). *SLFN11* is commonly inactivated by promoter hypermethylation (Gardner et al., 2017; Nogales et al., 2016). Therefore, *SLFN11* inactivation is potentially one of the prevalent mechanisms of epigenetic resistance to widely used anticancer drugs.

Insights in the molecular functions of SLFN11 have only been provided by a few recent studies (Marechal et al., 2014; Mu et al., 2016; Murai et al., 2016; Zoppoli et al., 2012). A connection between SLFN11 and replication stress is consistent with the co-immunoprecipitation of SLFN11 with RPA1 (Marechal et al., 2014). Mu et al. recently reported that SLFN11 is recruited to end-resected DNA lesions via RPA1 after CPT, and proposed that SLFN11 removes RPA complexes at late time points (24–48 hours after CPT treatment) while inhibiting homologous recombination. We also showed that SLFN11 induces lethal replication block in response to PARP inhibitors independently of ATR, and proposed that SLFN11 acts in parallel with the ATR-mediated S-phase checkpoint (Murai et al., 2016). However, the mechanistic details by which SLFN11 inhibits replication have until now remained unexplained. They are investigated in the present study.

RESULTS

SLFN11 persistently blocks replication independently from ATR in response to replication stress

Using isogenic (parental and *SLFN11*-deleted) cell lines derived from leukemia CCRF-CEM (Murai et al., 2016), we verified (Zoppoli et al., 2012) that SLFN11 drives cell killing by CPT, cisplatin and hydroxyurea (HU), but not by docetaxel (Taxol®), a tubulin inhibitor

(Figure S1B). Hereafter, to elucidate the molecular mechanisms by which SLFN11 kills cells, we first used CPT, which has well characterized effects on replication forks and readily activates the ATR-mediated S-phase checkpoint (Ray Chaudhuri et al., 2012; Seiler et al., 2007). We also combined CPT with ATR inhibitors (ATRi) (VE-821 or AZD6738) to determine whether SLFN11 is functionally linked with ATR. The ATR inhibitors were used at a concentration, which alone had little impact on cell cycle and viability (Figure S1C).

Short treatments with CPT (4 hours) induced potent inhibition of DNA replication regardless of SLFN11 (Figure 1A, panels c and d). Co-treatment with ATR inhibitors abrogated such replication inhibition in *SLFN11*-del cells while having limited effect in parental cells (Figure 1A, panels e and f). This SLFN11-mediated difference was not caused by differences in DNA damage as measured by γ-H2AX (Figure 1B), nor by differential ATR activation measured by CHK1 S345-phosphorylation, nor by differential CHK1 degradation that can inhibit resumption of replication (Zhang et al., 2009) (Figure 1C). Replication conferred by ATR inhibition in *SLFN11*-del cells was abrogated by roscovitine, a CDK/DDK inhibitor (Figure 1A, panels g and h) under conditions where roscovitine by itself did not inhibit replication (Figure S1C). The SLFN11-dependent replication block persisted at least 20 hours after drug removal (Figure S1D). These results were confirmed in the isogenic DU145 prostate cancer cell lines (Figure S1B and S1E–G). We conclude that SLFN11 blocks replication independently of ATR and that *SLFN11*-negative cells dominantly rely on ATR under replication stress. Consistently, in terms of cytotoxicity, the effect of ATR inhibition under CPT was highly prominent in *SLFN11*-del cells, but was limited in parental cells (Figure 1D). These results extend our recent finding with PARP inhibitors (Murai et al., 2016). They also demonstrate that ATR inhibitors overcome resistance to TOP1 inhibitors in *SLFN11*-negative cancer cells.

A day after continuous CPT treatment, *SLFN11*-del cells resumed replication while ATR remained activated. By contrast, parental cells remained replication-blocked regardless of ATR activation (Figure 1E–1F and S1E–S1F). The diminished CHK1 in CCRF-CEM parental cells may be related to the reduced S-phase cell population (Figure 1E), consistent with the reduction of cyclin A (Figure 1F). Additionally, CHK1 might be degraded through the proteasome pathway (Zhang et al., 2009). These results indicate that, while replication block by ATR is transient allowing cells to survive, the SLFN11-induced replication block persists until cells eventually die.

The ATPase Walker B motif of SLFN11 is required for SLFN11-mediated cell death and replication inhibition

Examination of the SLFN11 domains shows conserved putative DNA/RNA helicase and AAA domains (Zoppoli et al., 2012) (Figure S1H). Walker A motifs in AAA domains are responsible for ATP binding while ATP hydrolysis depends on the Walker B motifs (hhhhDE; where h represents hydrophobic amino acids). Mutation of the conserved glutamate (E) inactivates ATP hydrolysis (Weibezahn et al., 2003). To test the role of the Walker B motif of SLFN11, we overexpressed *SLFN11* in leukemia K562 cells, which have intrinsically low *SLFN11* expression (Figure S1A), and obtained clones expressing empty vector (+Vector), Flag-tagged wild-type *SLFN11* (+WT) and Flag-tagged Walker B motif-

mutant *SLFN11* (+E669Q). SLFN11 expression and nuclear localization were comparable in the wild-type *SLFN11* and E669Q *SLFN11* clones (Figure 1G–H). Yet, cells expressing wild-type *SLFN11* showed hypersensitivity to CPT, cisplatin and HU, while the Walker B-mutant (E669Q) *SLFN11* cells did not (Figure 1I).

CPT induced similar replication inhibition in the E669Q *SLFN11* and wild-type *SLFN11* cells (Figure 1J panels d–f). However, co-treatment with ATR inhibitor enabled replication in the E669Q cells but not in the wild-type *SLFN11* cells (Figure 1J panels g–i, S1H). These results imply that the ATPase Walker B motif of *SLFN11* is necessary for drug-induced cell killing and replication block.

SLFN11 is recruited via RPA1 to DNA damage sites and to the nuclear periphery where it inhibits replication

Immunofluorescence microscopy readily detects SLFN11 as a nuclear protein (Figures 1H and S2A–B) (Zoppoli et al., 2012). Biochemical fractionation showed that SLFN11 is recruited to chromatin within 2 hours of CPT or HU treatment (Figure 2A). To further explore SLFN11 chromatin binding, we performed confocal immunofluorescence experiments with pre-extraction. SLFN11 was mostly extracted in untreated cells whereas it formed nuclear foci in CPT-treated and CPT+ATRi-treated cells (Figure 2B and S2C). To examine the relationship between SLFN11 chromatin binding and replication inhibition, we labeled cells with the thymidine analog, 5-ethynyl-2′-deoxyuridine (EdU) during the last 30 min of 4 hour CPT treatments. In *SLFN11*-del cells treated with CPT, EdU staining was normalized by ATR inhibition (Figures 2B left and S2D). By contrast, in parental cells, the reduced EdU signal was not affected by ATR inhibition (Figures 2B right and S2D). Cells with the highest SLFN11 signal at 4 h with CPT and CPT+ATRi showed the lowest EdU signal while cells that still incorporated EdU had lower SLFN11 signal (Figure 2B right middle and lower panels). These results demonstrate that regardless of ATR activity, SLFN11 binds chromatin and blocks replication.

Based on the EdU staining patterns reflecting different phases of the cell cycle (Figure S2E), we estimate that ~40% of the untreated replicating cells were in mid-late S-phase regardless of SLFN11 (Figure S2F). Although CPT reduced EdU in both parental and *SLFN11*-del cells, the remaining EdU-positive cells were mostly (~95%) in early S-phase (Figure 2B and S2F). Addition of ATR inhibitor increased the mid-late S-phase population in *SLFN11*-del cells (~45%) but not in parental cells (~5%) (Figure S2F). From these results, we conclude that SLFN11 binds chromatin and blocks replication preferentially in mid-late S-phase.

The subcellular pattern of SLFN11 binding to chromatin was notable. SLFN11 foci were both in the nucleoplasm and at the nuclear periphery after CPT treatment independently of ATR (Figure 2B, green). A recent study showed that SLFN11 forms nuclear foci via RPA1 and is recruited to DNA damage sites in a CtIP-dependent manner (Mu, et al. 2016). To examine whether SLFN11 foci were formed at resected sites, we stained cells for SLFN11 and phosphorylated RPA2 (S4/S8, pRPA2), which marks resected DNA ends (Liaw et al., 2011). pRPA2 foci co-localized with SLFN11 (Figures 2C and S2G), and the overall intensity of SLFN11 and pRPA2 signals per cell were significantly correlated (Figure S2H). Yet, the SLFN11 foci at the nuclear periphery were largely negative for pRPA2 (Figures 2C

and S2G). The nuclear peripheral staining pattern of SLFN11 was also observed in the DU145 parental cells (Figure 2D, siControl CPT).

To characterize the SLFN11 foci at the nuclear periphery from the SLFN11-pRPA2 foci distributed within the nucleoplasm, we suppressed RPA1 or CtIP by siRNA transfection (Figure 2E). Knocking-down RPA1 suppressed CPT-induced SLFN11 and pRPA2 overall (Figure 2D and S2I), whereas CtIP knockdown reduced the SLFN11 foci in the nucleoplasm without affecting the peripheral SLFN11 foci (Figure 2D, siCtIP CPT). Consequently, the population of cells having SLFN11 signal exclusively at the periphery was significantly increased after CtIP knockdown (Figure 2F). These results demonstrate that SLFN11 is recruited by RPA1 both to the nuclear periphery and DNA damage sites, and that the SLFN11 foci at the nuclear periphery are independent of CtIP-mediated DNA end-resection.

SLFN11 is recruited to replication foci and binds the MCM replication helicase

To determine where in chromatin SLFN11 binds, we took advantage of the fact that E669Q SLFN11 is recruited to chromatin in a similar manner as wild-type SLFN11 (Figure 3A), while not inhibiting replication under CPT+ATRi (Figure 1J). In response to CPT and CPT +ATRi, wild-type SLFN11 formed foci both in the nucleoplasm and at the nuclear periphery with reduction of EdU foci in the K562 cells (Figure 3B left). E669Q SLFN11 showed a similar staining pattern as wild-type SLFN11. EdU labeling was reduced by CPT both in wild-type and E669Q SLFN11 cells (Figure 3B). However, ATR inhibition (CPT+ATRi) restored the EdU signals in E669Q SLFN11 cells. Notably, these Edu foci largely co-localized with the E669Q SLFN11 foci (Figure 3B bottom right). Approximately 90% of E669Q SLFN11 foci-positive cells were EdU-positive, while only ~3% of wild-type SLFN11 foci-positive cells were EdU-positive under CPT+ATRi (Figure 3C). These results demonstrate that SLFN11 binds replication foci independently of its ATPase domain, and that the ATPase domain of SLFN11 is required to block replication.

To identify interacting partner(s) of SLFN11, we performed immunoprecipitation coupled with mass spectrometry (IP-MS) using SLFN11 antibody, and compared the interacting proteins before and after CPT treatment (Figure 3D, Table S1–S2). As reported (Nogales et al., 2016), DHX9 (DExH-box helicase 9) was detected and the interaction was increased by CPT. MCM3, a component of the MCM replicative helicase, was also detected and its interaction with SLFN11 was increased by CPT (Figure 3D). These results were confirmed by co-immunoprecipitation using SLFN11, DHX9 and MCM3 antibodies (Figure 3D right panels). These findings show that, in addition to DHX9, SLFN11 interacts with the replication helicase MCM3.

SLFN11 is not involved in immediate fork slowing as ATR does, but inhibits activation of replication foci under replication stress

To examine whether SLFN11 acts immediately on elongating forks in response to CPT treatment, like ATR does (Josse et al., 2014), we performed DNA fiber analyses (Figure S3A). Without drug treatment, fork speed was similar in parental and *SLFN11*-del cells (Figure S3B). As reported (Seiler et al., 2007), CPT reduced fork speed within 30 minutes. ATR inhibition prevented the fork speed reduction induced by CPT both in parental and

SLFN11-del cells, and alone did not affect replication speed (Figure S3C). Consistent results were obtained by FACS analyses with BrdU pulse-labeling (Figure S3D). These results are notably different from those obtained after 4 hour treatments (see Figures 1A, 1J and S1E), and show that SLFN11 does not act immediately on replication fork elongation.

To test whether SLFN11 affects the activation of replication foci, cells were sequentially labeled with CldU (red) and IdU (green) for 30 min with an interval of 4 hours with or without drug treatment (Figure S3E) (Seiler et al., 2007). In untreated cells, about 50% of cells had distinct IdU replication foci in CldU-positive cells regardless of SLFN11 (Figure S3E–F). The isolated IdU foci-positive cell population was significantly reduced by CPT regardless of SLFN11. In *SLFN11*-del cells, addition of ATR inhibitor restored the isolated IdU foci, and further addition of the CDK inhibitor roscovitine reduced them, indicating that those foci were formed by origin firing under the control of CDK. By contrast, ATR inhibition failed to reactivate the IdU foci in parental cells (Figure S3E–F). These results show that SLFN11 blocks replication foci formation following replication stress independently of ATR.

SLFN11 blocks replication differently from ATR, downstream from CDC45 and PCNA loading

To determine which replication step is blocked by SLFN11, we analyzed the chromatin binding of CDC45, an essential and limiting factor for replication initiation and sustained activity of the MCM helicase complex (Aladjem and Redon, 2016; Fragkos et al., 2015). We labeled replication foci with a 30 min EdU pulse, and compared them with CDC45 and SLFN11 nuclear foci. In untreated cells, EdU and CDC45 foci were co-localized (Figure 4A) and their intensities correlated (Figure 4B). CPT profoundly reduced both the EdU and CDC45 signals independently of SLFN11 (Figures 4A–B and S4A). Inhibiting ATR restored both the EdU and CDC45 foci in *SLFN11*-del cells but only restored CDC45 signals in parental cells (Figures 4A–B, S4A–B). These CDC45 foci co-localized with SLFN11 (Figures 4A and S4B), indicating that SLFN11 binds where CDC45 also binds and blocks replication without interfering with the loading of CDC45 to replication foci.

PCNA loading, the next step after activation of the MCM helicase complex was also inhibited by CPT. Inhibition of ATR recovered the PCNA signals regardless of SLFN11 while EdU foci were only recovered in the *SLFN11*-del cells (Figures 4C–D and S4C). These findings were confirmed by Western blotting of chromatin fractions. CPT reduced CDC45 and PCNA protein levels similarly in parental and *SLFN11*-del cells (Figure S4D). The addition of ATR inhibitor restored both CDC45 and PCNA protein levels, and the addition of roscovitine inhibited this restoration regardless of SLFN11 (Figure S4D). Comparable results were obtained with K562+Vector and K562+WT cells (Figure S5A). Wild-type SLFN11 and E669Q SLFN11 also co-localized with CDC45 under CPT+ATRi treatment (Figure S5B). These results demonstrate that SLFN11 does not affect the loading of CDC45 and PCNA, and blocks replication in a different manner from ATR-CHK1, which inhibits the loading of CDC45 to replication foci.

SLFN11 blocks stressed replication forks carrying extended RPA filament

Next, we examined RPA loading generated by extended ssDNA segments due to uncoupling between the replicative MCM helicase and DNA polymerases or by DNA end-resection. Under normal conditions, replicating EdU positive cells did not show significant RPA2 foci, reflecting the coupling and proximity of the MCM helicase with replicative polymerases (Figure 4E). As CPT reduced the EdU signals, it induced RPA2 foci generated both by MCM-polymerase uncoupling at stressed replication foci and by end-resection at DNA damaged sites (Figure 4E).

In *SLFN11*-del cells, ATR inhibition induced additional RPA2 signal with diffuse staining pattern (Figures 4E–F and S4E–F) and co-localization with EdU (Figures 4E and S4F). This diffuse RPA2 pattern reverted to the dot pattern observed with CPT alone upon addition of roscovitine as EdU signals were reduced (Figure 4E). By contrast, in parental cells, the RPA2 dot pattern remained similar under the different treatments (CPT alone, CPT+ATRi or CPT+ATRi+Roscovitine) (Figure 4E). Additionally, more chromatin bound RPA2 was observed by Western blotting in *SLFN11*-del cells than parental cells (Figure S4D). Elevated chromatin-bound RPA2 was also enhanced in K562+Vector cells compared to K562+WT cells at 4 hours under CPT+ATRi treatment (Figures S5A). These results suggest that replication in *SLFN11*-del cells under CPT+ATRi is accompanied with extensive RPA loading within replication foci, while in parental cells, SLFN11 suppresses RPA loading by blocking replication.

SLFN11 opens chromatin in the vicinity of replication initiation sites under replicative stress

To test whether SLFN11 affects replication initiation, we mapped and quantified the initiation sites genome-wide using the nascent strand sequencing and abundance assay (NS-seq), which maps 500–2000 bp nascent strand DNA with RNA primers in the whole genome (Fu et al., 2014). Peak analysis using SICER algorithm revealed that replication initiation sites were enriched in promoter regions regardless of SLFN11 and drug treatment (Figure S6A). Approximately 90% of the peaks in *SLFN11*-del cells were co-located with peaks in parental cells regardless of drug treatment (Figures 5A and S6B). CPT reduced overall peak height regardless of SLFN11 (Figure 5A–B). Addition of ATRi (CPT+ATRi) restored peak heights both in *SLFN11*-del and parental cells (Figure 5A–B) under condition where replication measured by BrdU and EdU incorporation was suppressed selectively in parental cells (Figures 1A, 2B and 4). These results indicate that while ATR activation inhibits replication by halting replication initiation, SLFN11 blocks replication without affecting replication initiation.

To determine whether replication inhibition by SLFN11 is due to chromatin alterations, we performed ATAC-seq (Assay for Transposase-Accessible Chromatin with high throughput sequencing), which identifies accessible chromatin regions in the whole genome (Buenrostro et al., 2013). Peak analysis with SICER algorithm revealed that open chromatin regions were enriched in promoter regions regardless of SLFN11 and drug treatment (Figure S6C). The center of peaks in ATAC-seq was localized in the vicinity of the center of peak in NS-seq (Figure 5A and 5C, arrows). Approximately half of the peaks of NS-seq were co-localized

with the peaks of ATAC-seq in *SLFN11*-del and parental cells (Figure 5F). ATAC peaks (~70% of peaks) coincided in *SLFN11*-del and parental cells regardless of drug treatment (Figure 5C and S6D). While in *SLFN11*-del cells, peak height was not significantly changed by CPT, peak height as well as peak width were substantially increased in parental cells in response to CPT (Figure 5C). Peak analysis with MACS2 algorithm revealed that the average signal value from all peaks in parental (SLFN11-positive) cells was highly increased by CPT (59% and 51% compared to the control at 2 and 4 hours, respectively) (Figure 5D right). By contrast, in *SLFN11*-del cells the average change was only +7% and 0% at 2 and 4 hours CPT treatment, respectively (Figure 5D left). To examine whether chromatin opening by SLFN11 alters active histone marks (H3K4me3, K3K9ac and K3K27ac) (Buenrostro et al., 2013), we performed ChIP assay using anti-H3K9ac antibody. Figure 5E shows that the SLFN11-dependent chromatin opening was not accompanied with apparent change in H3K9ac. These results reveal that SLFN11 binding to chromatin results in chromatin opening at promoter sites in response to CPT.

Using our isogenic K562 cells, we tested whether chromatin opening by SLFN11 in response to CPT was ATPase-dependent. Representative initiation sites in K562 cells for the *HBB*, *JUNB* and *CTCF* genes (Fu et al., 2014; Martin et al., 2011) as well as *TOP1* promoter locus were opened in response to CPT treatment in K562-WT but not in K562-vector and −E669Q cells (Figure 5G). These results show that chromatin opening in the vicinity of initiation sites in response to replication stress requires the ATPase activity of SLFN11.

SLFN11 binds and blocks replication forks following CHK1 inhibition

To examine whether SLFN11 can be directly engaged by replication stress, we tested the clinical CHK1 inhibitor (CHK1i, LY2606368, Prexasertib) (King et al., 2015), which alone causes unscheduled origin firing by activating CDK/DDK (Petermann et al., 2010). CHK1i treatment for 4 hours induced SLFN11 binding to chromatin (Figure 6A–B) and increased the chromatin binding of CDC45 in both parental and *SLNF11*-del cells (Figure 6A and C). Notably, replication foci (EdU incorporation) were inactivated in parental cells but not in the *SLFN11*-del cells (Figure 6A and D). In CHK1i-treated cells, SLFN11 foci co-localized with CDC45 (Figure 6A) and the intensity of the SLFN11 and CDC45 signals per cell were significantly correlated (Figure 6E). Also, cells with high SLFN11 signal tended to have low EdU (Figure 6A and 6F). The binding of SLFN11 and CDC45 to chromatin and their co-localization in response to CHK1i treatment were also observed in K562+WT and K562+E669Q cells (Figure S7). These results demonstrate that SLFN11 is recruited and blocks stressed replication forks following unscheduled origin firing by CHK1 inhibition without interfering with CDC45 loading.

Next, we measured RPA2 loading to chromatin, which takes place during unscheduled origin firing by CHK1i (Syljuasen et al., 2005). In parental cells, RPA2 foci formed in response to CHK1i (Figure 6G–H) with partial (~20%) co-localization of CDC45 and RPA2 signals (Figure 6I). In *SLFN11*-del cells, RPA2 staining was more diffuse and extensive (Figure 6G–H), and largely (~50%) overlapped with CDC45 (Figure 6I). These results obtained with the CHK1i Prexasertib are consistent with those observed with the CPT+ATRi

combination (Figures 4E–F and S4F). They suggest that SLFN11 stops extensive loading of RPA while blocking replication.

Co-localization of EdU and E669Q SLFN11 foci (Figure 3B), co-localization of SLFN11 and CDC45 foci under replication stress (Figure 4, 6 and S7) and interaction with MCM3 and SLFN11 under CPT treatment (Figure 3) imply that SLFN11 binds to stressed replication forks. To determine whether SLFN11 was directly associated with replication forks, we performed isolation of proteins on nascent DNA (iPOND) (Ribeyre et al., 2016; Sirbu et al., 2012) using the CHK1i, which does not fully abrogate EdU incorporation (see Figure 6D). SLFN11, CDC45 and PCNA were enriched on nascent DNA under CHK1i treatment in the three cell lines tested (Figure 6J). These results establish that SLFN11 binds to nascent DNA under replication stress where CDC45 and PCNA also accumulate. Hence, SLFN11 blocks replication at stressed replication forks both in response to CPT and to the CHK1i Prexasertib.

DISCUSSION

Understanding of the molecular mechanism by which SLFN11 sensitizes cancer cells to DNA-targeted drugs have only begun to emerge with two recent publications showing that SLFN11 binds resected DNA ends via RPA1 in response to CPT (Mu et al., 2016) and that SLFN11 blocks replication independently of ATR (Murai et al., 2016). Both studies analyzed the effect of SLFN11 at late time points (24 and 48 h after drug treatment), whereas the current study examines the early effects of SLFN11 in response to replication stress induced by stalled TOP1, HU and the clinical CHK1 inhibitor Prexasertib. We show that: 1/SLFN11 is recruited to stressed replication forks beyond DNA damaged sites; 2/ SLFN11 binds nascent DNA and interacts with MCM3; 3/SLFN11 blocks replication without interfering with initiation and CDC45 in a different manner from ATR; and 4/the ATPase-Walker B domain of SLFN11 is critical for chromatin opening and replication arrest but not for SLFN11 recruitment to chromatin; all of which happen within 4 hours of replication stress.

Our working model of SLFN11 molecular function at stressed replication forks is illustrated in Figure 7. Under normal conditions, replication forks only form short ssDNA segments coated with RPA, and SLFN11 does not gain access to forks (Figure 7A). Under CPT treatment (Figure 7B), DNA breaks activates ATR and slow down replication (Figure S3) leading to the uncoupling of the MCM helicase complex and DNA polymerases at stressed replicons (Figure 7B pathway 1). Activated ATR and CHK1 halt replication initiation by inhibiting the loading of CDC45 (Figure 7B pathway 2; Figure 4A). SLFN11 binds both resected DNA ends (Figure 2D; not shown in detail in Figure 7B left) and stressed replication forks via RPA1, where it interacts with MCM3, opens chromatin and blocks replication (Figure 7B pathway 1). CPT+ATRi or CHK1i induce unscheduled origin firings with extended RPA loading (Figures 4E, 6G and 7C). As SLFN11 does not inhibit replication initiation (Figures 4 and 5), stressed replication forks with RPA filaments are generated, recruiting SLFN11, which blocks fork progression (Figure 7C top). In the absence of SLFN11, uncoupling of the replication helicase and polymerases keeps progressing, resulting in extensive RPA loading (Figure 7C bottom). We demonstrate that

the ATPase activity of SLFN11 is required for SLFN11 to block fork progression and to open chromatin. As SLFN11 opens chromatin across replication initiation sites, a plausible scenario is that once SLFN11 binds stressed replication forks, SLFN11 may unwind DNA ahead of the MCM helicase, which blocks the MCM complex and fork progression (Figure 7B and C).

Our results add to recent findings of Mu et al. focusing on the role of SLFN11 at DNA damaged sites and proposing that the recruitment of SLFN11 to chromatin inhibits checkpoint maintenance and homologous recombination (HR) by promoting the destabilization of the RPA-ssDNA complex. Mu et all derived their conclusion from the fact that RPA2 loading, although comparable at 3 hours after CPT treatment, was reduced further in *SLFN11*-positive cells at 24 and 48 hours compared to SLFN11-negative cells. These late effects can be explained as secondary to SLFN11-mediated-replication block. Indeed, HR would not occur if replication is blocked because it requires sister chromatids and active polymerases. Furthermore, we showed less RPA recruitment to chromatin at 4 hours after CPT+ATRi or CHK1i treatment, which we interpret as a result of replication block by SLFN11 (Figure 4E and 6G). Yet, it is not excluded that SLFN11 could act by a dual mechanism: direct removal of RPA and inhibition of RPA loading through replication block. Another point of discussion is the functional difference between our Walker B mutants (E669Q SLFN11) and the reported K605M/D668A double mutant of Mu et al. Our E669Q mutant is a classical Walker B motif mutant, which is predicted to selectively lose ATP hydrolysis, and we show that it retains chromatin binding activity but loses SLFN11 functional activities (chromatin opening and replication arrest). Further studies are warranted to clarify why the reported K605M/D668A was apparently normal. The different mutation sites could drive the differential impact on SLFN11 function. Finally, Mu et al. studied SLFN11 chromatin binding using Flag antibody and their self-made rabbit polyclonal antibody raised against 1–300 amino acid. We used mouse monoclonal SLFN11 (D-2) antibody raised against 154–203 from Santa Cruz Biotechnology. The different staining patterns can be derived from the different recognition region and specificity between antibodies.

RPA exhaustion has been proposed as a death mechanism to replication stress (Toledo et al., 2013), which was described for *SLFN11*-negative U2OS and DLD-1 cells (Figure S1A). Our results show that *SLFN11*-positive cells are killed without RPA exhaustion and that replication is blocked independently of ATR-dependent CHK1 degradation (Zhang et al., 2009). Hence, cell killing and replication blocking effect by SLFN11 through chromatin remodeling appears unprecedented. Why has such a dominant ATR-independent replication blocking mechanism by SLFN11 been missed until now? A plausible answer is that commonly used cancer cell lines such as HCT116, U2OS, HeLa, MCF-7, MDA-MB231, DLD-1 and HT-29 are all *SLFN11*-negative (Figure S1A). Similar to *TP53*, which is among the most frequently inactivated genes in cancers (~50%) and a critical tumor suppressor involved in G1 arrest and apoptosis, SLFN11 is inactivated in ~50% of cancer cell lines. This may allow such cells to progress through the cell cycle in spite of replication stress without being arrested and killed in S-phase. A selective pressure in favor of SLFN11 inactivation is consistent with its epigenetic silencing in many in cancer cells (Nogales et al., 2016). Therefore, SLFN11 potentially functions as a guardian of the genome, and its

inactivation in cancer cells may be a key mechanism for their growth under replication stress. Further studies are warranted to determine whether SLFN11 also serves as a barrier to viral replication and infections.

STAR METHODS

Detailed methods are provided in the online version of this paper and include the following:

KEY RESOURCES TABLE

REAGENT or RESOURCE	SOURCE	IDENTIFIER
Antibodies		
Mouse monoclonal anti-phospho (S139)-H2AX (JBW301)	Millipore	cat# 05-636
Rabbit monoclonal anti-phospho (S345)-CHK1 (133D3)	Cell Signaling Technology	cat# 2348S
Mouse monoclonal anti-CHK1 (G-4)	Santa Cruz	cat# sc-8408
Mouse monoclonal anti-SLFN11 (D-2) (special request, 200 μg/100 μl)	Santa Cruz	cat# sc-515071X
Mouse monoclonal anti-SLFN11 (E-4)	Santa Cruz	cat# sc-374339
Mouse monoclonal anti-BrdU FITC (B44)	Becton Dickinson	cat# 347583
Rabbit polyclonal anti-phospho (S4/S8)-RPA2	BETHYL	cat# A300-245A
Rabbit monoclonal anti-RPA70 (RPA1) (C24F2)	Cell Signaling Technology	cat# 2193S
Rabbit monoclonal anti-CtIP (D76F7)	Cell Signaling Technology	cat# 9201S
Rabbit monoclonal anti-CDC45 (D7G6)	Cell Signaling Technology	cat# 11881S
Mouse monoclonal anti-RPA2 (Ab-3)	Oncogene	cat# NA19L-100UG
Rabbit monoclonal anti-RPA70 (RPA1) (C24F2)	Cell Signaling Technology	cat# 2193S
Rabbit polyclonal anti-cyclin A (C-19)	Santa Cruz	cat# sc-596
Mouse monoclonal anti-BrdU (B44)	Becton Dickinson	cat# 347580
Rat monoclonal anti-BrdU [BU1/75(ICR1)]	Abcam	cat# ab6326
Cy3 affiniPure F(ab′)$_2$ fragment donkey polyclonal anti-Rat IgG	Jackson Immuno Research	cat# 712-166-153
Rabbit polyclonal anti-Histone H3	Millipore	cat#07-690
Rabbit monoclonal anti-GAPDH	Cell Signaling Technology	cat# 2118S
Mouse monoclonal anti-PCNA (PC10)	Santa Cruz	cat# sc-56
Rabbit polyclonal anti-DHX9	BETHYL	cat# A300-855A
Rabbit polyclonal anti-MCM3	BETHYL	cat# A300-192A
Rabbit polyclonal anti-MCM2	BETHYL	cat# A300-191A
Rabbit polyclonal anti-ORC2	Novus	cat# NBP1-46175
Rabbit polyclonal anti-Histone H3 (acetyl K9)	abcam	cat# ab4441
Normal rabbit IgG	Santa Cruz	cat# sc-2027
Alexa Fluor 488 goat anti-mouse IgG	Molecular Probes	cat# A11001
Alexa Fluor 568 goat anti-rabbit IgG	Molecular Probes	cat# A11036
ECL anti-mouse IgG, horseradish peroxidase linked whole antibody (from sheep)	GE Healthcare	cat# NA931V
ECL anti-rabbit IgG, horseradish peroxidase linked whole antibody (from donkey)	GE Healthcare	cat# NA934V
Chemicals, Peptides, and Recombinant Proteins		

REAGENT or RESOURCE	SOURCE	IDENTIFIER
Camptothecin (CPT)	Developmental Therapeutics Program (NCI/NIH)	NSC#94600
cis-Diammineplatinum(II) dichloride	Sigma-Aldrich	cat# P4394
Hydroxyurea	Developmental Therapeutics Program (NCI/NIH)	NSC#32065
Paclitaxel	Sigma-Aldrich	cat# T7402
5-Bromo-2′-deoxyuridine (BrdU)	Calbiochem	cat# 203806
5-Chloro-2′-deoxyuridine (CldU)	Sigma-Aldrich	cat# C6891
5-Iodo-2′-deoxyuridine (IdU)	Fluka	cat# 57830
5-ethynyl-2′-deoxyuridine (EdU)	Molecular probes	cat# A10044
VE-821 (ATR inhibitor)	Developmental Therapeutics Program (NCI/NIH)	NSC#761070
AZD6738 (ATR inhibitor)	Developmental Therapeutics Program (NCI/NIH)	NSC#780249
Roscovitine (Seliciclib, CYC202)	Selleckchem	cat# S1153
LY2606368 (CHK1 inhibitor)	Developmental Therapeutics Program (NCI/NIH)	NSC#758257
cOmplete Mini, EDTA-free (protease inhibitor cocktail)	Roche	cat# 11836170001
Critical Commercial Assays		
ATPlite 1step luminescence assay system	PerkinElmer	cat# 6016739
Click-iT Plus EdU Alexa Fluor 647 Imaging Kit	Invitrogen	cat# C10640
Subcellular Protein Fractionation Kit for Cultured Cells	Thermo Scientific	cat# 78840
QuikChange II XL site-directed mutagenesis kit	Agilent Technologies	cat# 200521
Nextera DNA Library Preparation Kit	Illumina	cat# 15028212
ChIP-IT Express	Active Motif	cat# 53008
ChIP DNA Clean & Concentrator	ZYMO RESEARCH	cat# D5205
FastStart Universal SYBR Green Master (Rox)	Roche	cat# 21966100
Deposited Data		
Immunoprecipitation coupled to mass spectrometry for SLFN11 interacting proteins	This paper	Table S1 and S2
ATAC-seq data	This paper	GSE101512
Nascent strand DNA-seq data	This paper	GSE101515
All the unprocessed and uncompressed imaging data (microscopy, gels, blots and FACS data)	This paper	Mendeley Data at: h datasets/sgtswby25 a=6eda2bb4-9cd0-4
Experimental Models: Cell Lines		
Human: prostate cancer DU145 cells	Developmental Therapeutics Program (NCI/NIH)	
Human: leukemia CCRF-CEM cells	Developmental Therapeutics Program (NCI/NIH)	

REAGENT or RESOURCE	SOURCE	IDENTIFIER
Human: leukemia K562 cells	Developmental Therapeutics Program (NCI/NIH)	
DU145 SLFN11 knockout cells	(Murai et al., 2016)	
CCRF-CEM SLFN11 knockout cells	(Murai et al., 2016)	
K562 vector overexpressing cells	(Murai et al., 2016)	
K562 wild-type SLFN11 overexpressing cells	(Murai et al., 2016)	
K562 E669Q SLFN11 overexpressing cells	This paper	
Oligonucleotides		
siRNA targeting Human CtIP (RBBP8), SMART pool 5′-GGAGCUACCUCUAGUAUCA-3′ 5′-GAGGUUAUAUUAAGGAAGA-3′ 5′-GAACAGAAUAGGACUGAGU-3′ 5′-GCACGUUGCCCAAAGAUUC-3′	Dharmacon	cat# L-011376-00-0
siRNA targeting Human RPA1, SMART pool 5′-CCCUAGAACUGGUUGACGA-3′ 5′-AAGCAGGAAUUAUGUCGUA-3′ 5′-CCACUGUGAUGGACGUGAA-3′ 5′-CAGAAUGGAAGCUCGGGAA-3′	Dharmacon	cat# L-015749-01-0
siRNA targeting Non-targeting pool	Dharmacon	cat# D-001810-10-0
Forward primer to amplify SLFN11cDNA: 5′-ATCGGATCCGCGGCCAACATGGAGGCAAATCAGTGC-3′	IDT oligo	N/A
Reverse primer to amplify SLFN11cDNA: 5′- ATTGTCGACGCGGCCCTACTTATCGTCGTCATCCTTGTAATCATGGCCACCCCACGGA-3′	IDT oligo	N/A
Primer for the mutagenesis of SLFN11 5′-CGTCATTGACGAAGCTCACAATTTCCGTACTGAAGATG-3′	IDT oligo	N/A
Primers for qPCR	Table S4	N/A
Recombinant DNA		
pCDH-EF1-MCS-PGK-copGFP lentiviral expression vector	System Biosciences	
pPACKH1 lentivector packaging plasmids	System Biosciences	
Software and Algorithms		
GraphPad Prism 7 (software for drawing graphs and statistics analysis)	GraphPad	
Image J (software for mage analysis)	NIH	
ZEN (software for microscopy image analysis)	ZEISS	
CellMiner (web application for analysis of NCI-60 database)	Genomics & Bioinformatics Group/ Developmental Therapeutics Branch/ Laboratory of Molecular Pharmacology/CCR/NCI/ NIH	https://discover.nci.
Genomatix genome analyzer		https://genomeanaly
Integrated Genome Viewer	Broad Institute	http://software.broa
Colocalization Analysis of Genome Features (Coloweb)		http://projects.insili

CONTACT FOR REAGNET AND RESOURCE SHARING

Further information and requests for reagents may be directed to and will be fulfilled by Lead Contact Yves Pommier (pommier@nih.gov).

METHODS DETAILS

Cell culture—DU145, CCRF-CEM, and K562 cell lines were grown in RPMI medium 1640 (1x, Gibco, 11875-093) added with 10% Fetal Bovine Serum (Gemini, 100–106) and 1% penicillin-streptomycin (Gibco, 15140-122) at 37°C in 5% CO_2.

Viability assay—To measure the sensitivity of cells to drugs, cells were continuously exposed to various concentrations of the drugs. Two thousand CCRF-CEM cells, and six hundred K562 cells were seeded in 384-well white plates (Perkin Elmer Life Sciences, 6007680) in 40 μl of medium per well. One thousand five hundred DU145 cells were seeded in 96-well white plates (#6005680 Perkin Elmer Life Sciences, 6005680) in 100 μl of medium per well. Cells were incubated for 72 hours in triplicate. Cellular viability was determined using the ATPlite 1-step kits (PerkinElmer). Briefly, 20 μl and 50 μl ATPlite solution was added in 384-well plates per well and in 96-well plates per well, respectively. After 5 min, luminescence was measured with an EnVision 2104 Multilabel Reader (PerkinElmer). The ATP level in untreated cells was defined as 100%. Viability (%) of treated cells was defined as ATP treated cells/ATP untreated cells x 100.

Immuoblotting and quantification—To prepare whole cell lysates, cells were lysed with CellLytic™M lysis reagent (C2978, Sigma-Aldrich). After thorough mixing and incubation at 4°C for 30 min, lysates were centrifuged at 15,000 g at 4°C for 10 min, and supernatants were collected. To prepare chromatin bound subcellular fraction, we followed the protocol of Subcellular Protein Fractionation Kit from Thermo Scientific (78840). Samples were mixed with tris-glycine SDS sample buffer (Novex, LC2676) and loaded onto Novex tris-glycine gels (Novex). Blotted membrane was blocked with 5% bovine serum albumin (BSA) (Sigma-Aldrich. A9418) in phosphate-buffered saline (PBS) with 0.1% tween-20 (PBST). The primary antibodies were diluted in 5% BSA/PBST by 1:3000 for phospo-S345-CHK1, CHK1, phspho-S4/S8-RPA2, RPA1, CtIP, CDC45, DHX9, cyclin A and ORC2, and 1:10000 for phospho-S139-H2AX, SLFN11 (D-2), RPA2, Histone H3, GAPDH, PCNA, MCM3 and MCM2. The secondary antibodies were diluted in 5% non-fat milk by 1:10000. Quantification of band intensity was done using ImageJ software. A proper size of square that was slightly larger than blot bands was set, and used to measure the mean intensity of each band. The square size was consistent through the experiment for each antibody. Intensity of background was subtracted, and the intensity of each control sample was set as 1.

Cell cycle analysis by flow cytometry—Cells were incubated with 10 μM 5-bromo-2′-deoxyuridine (BrdU) for 1 hour except for the Figure S3D (incubated for 30 min) before fixation with 70% ethanol. BrdU was detected by anti-BrdU FITC (Becton Dickinson, 347583), or anti-BrdU (Becton Dickinson, 347580) followed by Alexa Fluor 488 goat anti-mouse IgG (Molecular Probes, A110011). Propidium iodide (PI) was used to measure DNA content. Data were collected with BD LSRFortessa (Becton Dickinson) and the data was analyzed with BD FACSDiva software (Becton Dickinson).

Immunofluorescence analysis with or without EdU labeling—If needed, cells were incubated with 10 μM 5-ethynel-2′-deoxyuridine (EdU) for 30 min just before

collected. Cells were deposited onto slide glasses (Superfrost Plus Microscope Slides precleaned, Fisher Scientific, 12-550-15) by cytospin. Except for the Figure 1H, the deposited cells were pretreated with cold 0.1% Triton-X 100/PBS for 1 min on ice, and then fixed with 4% paraformaldehyde in PBS for 10 min. For the Figure 1H, the deposited cells were fixed with 4% paraformaldehyde for 10 min followed by permeabilization with 0.1% Triton-X 100/PBS for 15 min. Next, when EdU detection is necessary, cells were incubated with 5% BSA/PBST for 10 min, and then incubated with Click-IT Plus reaction cocktail for 30min (Invitrogen, C10640) followed by washing steps with 5% BSA/PBST twice and incubation with 5% BSA/PBST for 30 min (blocking step). When EdU detection is not necessary, cells were incubated with 5% BSA/PBST for 30 min (blocking step) after fixation. After the blocking step, cells were incubated for overnight with primary antibodies/5% BSA/PBST in moisture chamber at 4°C by 1:300 dilution for phospho-S4/S8-RPA2, CDC45, RPA2, PCNA, and 1:1000 dilution for phospho-S139-H2AX and SLFN11 (D-2). After washing with PBST, the cells were incubated with proper second antibodies/5% BSA/PBST by 1:1000 dilution for 2–4 hours. After washing with PBST, cells were mounted with Vectashield with DAPI (VECTOR, H-1200). Images were captured with a Zeiss LSM 780 or a Zeiss LSM 710 confocal microscope. Slides should be protected from light throughout the process. Because EdU signal (Alexa Fluor 647) was easily weaken by its emission light, capturing area were decided by DAPI image, and were not close each other.

Data analysis of immunofluorescence microscopy images—Signal intensity in each cell was measured using ImageJ software. A proper sized circle that was slightly larger than a regular cell size was set. The same circle was used to measure the mean intensity of each signal throughout an experiment in isogenic cell lines. The individual signals and/or correlation signals were plotted. The profile of signal distribution data in Figure 2C and 2D, and co-localization coefficient data (Figure 6I) were obtained using ZEN software. The data was transferred to GraphPad Prism 7 software, and illustrated. We set proper threshold at 20 for both CDC45 and RPA2 based on the background signal (i.e. we excluded background signal by setting the threshold at 20). Colocalization coefficient CDC45, which represents the faction of CDC45 signal overlapping with RPA2 signal in total CDC45 signal, was calculated from whole captured images (130 μm × 130 μm) containing ~50 cells/image.

DNA fiber analysis—We measured replication fork progression as described before (Ray Chaudhuri et al., 2012) with some modification. DU145 parental and *SLFN11*-del cells were labeled with 30 μM CldU for 30 min, washed quickly and exposed to 250 μM IdU with or without drug(s) for another 30 min. Cells were collected, and resuspended in PBS. Cells were then lysed with lysis buffer (200 mM TrisHCl pH 7.4, 50 mM EDTA, 0.5% SDS), and DNA fibers stretched onto glass slides (Superfrost Plus Microscope Slides precleaned, Fisher Scientific, 12-550-15) as described. The fibers were denatured with 2.5 M HCl for 1 h, washed with PBS and blocked with 2% BSA in PBST for 30 min. Labeled DNA with CldU and IdU were stained with anti-BrdU antibodies recognizing CldU and IdU, respectively. Anti-mouse Alexa 488 and anti-rat Cy3 were used for second antibodies. Images were captured with a Zeiss LSM 780 or a Zeiss LSM 710 confocal microscope. Fiber length was measured using ImageJ software.

Immunofluorescence analysis of dual DNA labeling—CCRF-CEM parental and *SLFN11*-del cells were labeled with 30 μM CldU for 30 min before treatment. After washing cells with cold PBS, cells were immediately labeled, or labeled 3.5 hours later with 250 μM IdU for 30 min. Meantime, cells were untreated or treated with drugs for 4 hours before fixation. Cells were deposited on slide glass by cytospin. Cells were fixed with 4% paraformaldehyde/PBS for 15 min, then put in 100% methanol at −20 °C for 15 min. DNA was denatured with 2N HCl/0.5% triton-100X/H_2O for 60 min, and then blocked with 5% BSA/PBST for 30 min. The same primary and secondary antibodies as DNA fiber analysis were used. Images were captured with a Zeiss LSM 780 or a Zeiss LSM 710 confocal microscope. CldU (red) positive cells were classified into early S or mid-late S-phase cells based on the staining pattern (Figure S2E). The number of CldU (red) positive cells in mid-late S-phase were counted, and the number of cells having >10 isolated IdU (green) foci (new replication forks) in the CldU positive cells were also counted manually.

Generation of *SLFN11*-deleted cells—*SLFN11*-deleted cells in DU145 and CCRF-CEM cell lines were generated by CRISPR/Cas9 methods, and the detail are described before (Murai et al., 2016).

Generation of *SLFN11*-overexpressing cells—*SLFN11* cDNA was amplified using the forward primer (5′-ATCGGATCCGCGGCCAACATGGAGGCAAATCAGTGC-3′) and the reverse primer with the sequence for the Flag tag (5′-ATTGTCGACGCGGCCCTACTTATCGTCGTCATCCTTGTAATCATGGCCACCCCACG GAA-3′) and cloned into pCDH-EF1-MCS-PGK-copGFP lentiviral expression vector (System Biosciences) by In-Fusion HD cloning kit (Clontech). SLFN11 mutant (E669Q) was generated using the primer (5′-CGTCATTGACGAAGCTCACAATTTCCGTACTGAAGATG-3′) and QuikChange II XL site-directed mutagenesis kit (Agilent Technologies), and the mutation was validated by sequence analysis. The lentiviral *SLFN11*-expressing vector and the pPACKH1 lentivector packaging plasmids were co-transfected into 293TN cells (System Biosciences) and the viral particles were collected to infect K562 cells with Transdux™ (System Biosciences). The *SLFN11*-expressing cells with GFP expression were sorted using a Fluorescence Activated Cell Sorter (FACS).

siRNA transfection—Gene-specific siRNAs (mix of four sequences) for human RPA1 (L-015749-01-0005), human CtIP (L-011376-00-0005), and negative control siRNA (D-001810-10-05) were products of Dharmacon. Ten nanomolar of each siRNA was transfected to DU145 cells with Lipofectamin RNAiMAX Reagent (13778, Invitrogen) according to the manufacturer's instructions. Culture medium was changed 6–8 hours after the transfection. Two days after the transfection, cells were subjected to immunofluorescence analysis and the whole cell lysate were analyzed by Western blotting.

Immunoprecipitation (IP) and IP coupled to mass spectrometry (IP-MS)—DU145 parental cells were untreated or treated with 100 nM CPT for 1 hour, and 1×10^7 cells were collected. Cells were re-suspended with 1 ml buffer A (10 mM HELES, 10 mM KCl, 1.5 mM MgCl2, 0.34M sucrose, 10% Glycerol, 0.1% TritonX, 1 mM DTT, protease

inhibitor in H_2O), and incubated on ice for 10 min. After centrifuge, the pellet was resuspended with 500 μl buffer B (3 mM EDTA, 1 mM DTT, 0.2 mM EGTA, protease inhibitor in H_2O), and incubated for 45 min at 4°C with agitation. After centrifuge, the supernatant (nuclear soluble fraction) was collected, and the pellet (chromatin fraction) was resuspended in 500 μl buffer A with 300 mM NaCl and 2 μl benzonase nuclease (Sigma-Aldrich, E8263), and incubated on ice for 20 min. The chromatin fraction was sonicated 6 times (30 sec each, 25% power, QSONICA) at 4°C, and incubated on ice for 10 min. The nuclear soluble fraction and the chromatin fraction were mixed, and centrifuged at maximum speed. The supernatant (nuclear fraction) was transferred to a new tube, and added 4 μg of SLFN11 (E-4) antibody, MCM3 antibody or DHX9 antibody and incubated for 2.5 hours at 4°C with agitation. In another tube, 25 μl of protein A/G magnetic beads (Pierce Thermo Scientific, 88802) was mixed with 500 μl buffer A and kept on ice. After the 2.5-hours incubation, the beads in buffer A was added to the nuclear fraction, and incubated for one hour at 4°C. The beads were washed with 1 ml of buffer A five times, and the IP samples were collected with 50 μl Laemmli buffer. The IP samples were analyzed by Western blotting and by mass spectrometry.

For mass spectrometry, interacting proteins were fractionated by SDS-PAGE and five intense bands (see Mendeley Data) were cut and then in-gel digested with trypsin (Thermo) overnight at 37 °C. The peptides were extracted following cleavage and lyophilized. The dried peptides were solubilized in 2% acetonitrile, 0.5% acetic acid, 97.5% water for mass spectrometry analysis. They were trapped on a trapping column and separated on a 75 μm × 15 cm, 2 μm Acclaim PepMap reverse phase column (Thermo Scientific) using an UltiMate 3000 RSLCnano HPLC (Thermo Scientific). Peptides were separated at a flow rate of 300 nL/min followed by online analysis by tandem mass spectrometry using a Thermo Orbitrap Fusion mass spectrometer. Peptides were eluted into the mass spectrometer using a linear gradient from 96% mobile phase A (0.1% formic acid in water) to 55% mobile phase B (0.1% formic acid in acetonitrile) over 30 minutes. Parent full-scan mass spectra were collected in the Orbitrap mass analyzer set to acquire data at 120,000 FWHM resolution; ions were then isolated in the quadrupole mass filter, fragmented within the HCD cell (HCD normalized energy 32%, stepped ± 3%), and the product ions analyzed in the ion trap. Proteome Discoverer 2.0 (Thermo) was used to search the data against human proteins from the UniProt database using SequestHT. The search was limited to tryptic peptides, with maximally two missed cleavages allowed. Cysteine carbamidomethylation was set as a fixed modification, and methionine oxidation set as a variable modification. The precursor mass tolerance was 10 ppm, and the fragment mass tolerance was 0.6 Da. The Percolator node was used to score and rank peptide matches using a 1% false discovery rate.

Nascent strand abundance assay (Nascent strand DNA-seq; NS-seq)— Replication origins were identified using the nascent-strand sequencing and abundance assay (Martin et al., 2011). In brief, twenty million of CCRF-CEM parental and *SLFN11*-del cells were treated with DMSO, CPT (100 nM), or CPT (100 nM) and VE-821 (2 μM) for four hours. DNA fractions (0.5–2 kb) were isolated using DNA fractionation on a 5–30% neutral sucrose gradient. 5′ single strand DNA ends were phosphorylated by T4 polynucleotide kinase (NEB) and then treated with lambda-exonuclease (NEB) to remove genomic DNA

fragments that lacked the phosphorylated RNA primer. After RNase treatment, purified single stranded nascent DNA were random-primed using the Klenow and DNA Prime Labeling System (Invitrogen). Double-stranded nascent DNA (1 μg) was sequenced using the Illumina genome analyzer II (Solexa).

Assay for Transposase-Accessible Chromatin with high throughput sequencing (ATAC-seq)—Genome-wide mapping of chromatin accessibility was done by following the published method (Buenrostro et al., 2013). Briefly, fifty thousand CCRF-CEM parental and *SLFN11*-del cells were treated with DMSO or CPT (100 nM) for 2 and 4 hours. K562-Vector, −WT and −E669Q cells were treated with DMSO or CPT (1 μM) for 4 hours. To prepare nuclei, cells were lysed using cold lysis buffer (10 mM Tris-Cl, pH 7.4, 10 mM NaCl, 3 mM MgCl2 and 0.1% IGEPAL CA-630). Immediately following the nuclei preparation, the pellet was re-suspended in the transposase reaction mix [25 μl 2x TD buffer, 2.5 μl Transposase (Illumina) and 22.5 μl of nuclease free water], and incubated for 30 minutes at 37 °C. Directly following transposition, the sample was purified using a DNA Clean and Concentrator-5 (ZYMO RESEARCH) and eluted with 25 μl of DNA elution buffer. Following purification, we amplified library fragments using 1x NEBnext PCR master mix and 1.25 μM of custom Nextera PCR primers 1 and 2, using the following PCR conditions: 72°C for 5 minutes, 98°C for 30 seconds, followed by thermo-cycling at 98°C for 10 seconds, 63°C for 30 seconds and 72°C for 1 minute. We amplified the full libraries for 5 cycles, after 5 cycles we took an aliquot of the PCR reaction and added 10 μl of the PCR cocktail with Syber Green at a final concentration of 0.6x. We ran this reaction for 20 cycles, to determine the additional number of cycles needed for the remaining 45 μL reaction. Libraries were amplified for a total of 10–12 cycles and purified using a PCRClean DX yielding a final library concentration of ~30 nM in 20 μl.

Chromatin immunoprecipitation (ChIP) assay—Twenty-five million CCRF-CEM parental and *SLFN11*-del cells were treated or untreated with CPT (100 nM) for 4 hours. ChIP assay was done by following the instruction manual of ChIP-IT Express (Active Motif). Briefly, cells were fixed with 1% formaldehyde in medium for 10 min at room temperature. Fixation was stopped with x1 glycine/PBS. Cells were lysed with lysis buffer with proteinase inhibitor cocktail and PMSF, and homogenized 60 times by small tight homogenizer. Cell pellets were re-suspended with sharing buffer, and sonicated by the following settings: pulse 20 s pulse, 40 s pause, amplitude 25%, repeat 5 times (QSONICA Sonicator, ultrasonic processor). Five %/volume of each sample was saved as input. The left of the supernatant was incubated with 2 μg antibody (H3K9ac or normal rabbit IgG) and protein G beads for overnight at 4°C. After reversing cross-link and proteinase K treatment, immunoprecipitated DNA was purified with ChIP DNA Clean & concentrator (ZYMO Research) according to the manual. Quantitative PCR was done using FastStart Universal SYBR Green Master (Roche) and ABI PRISM 7900TH.

Isolation of proteins on nascent DNA (iPOND)—iPOND was done by following and modifying the published methods (Ribeyre et al., 2016; Sirbu et al., 2012). Briefly, one hundred million cells (K562-WT, K562-E669Q and CCRF-CEM parental cells) were treated with DMSO or CHK1i (LY2606368, 100 nM) for 2 hours, and labelled with EdU during the

last 10 min before collecting cells. Cells were fixed with 2% formaldehyde/PBS for 10 min at room temperature, and the fixation was terminated with 250 mM glycine/PBS. After the fixation, all the procedures were done on ice using pre-chilled buffers. Cells were permeabilized with 0.25% Triton X/PBS for 30 min followed by click reaction (10 mM sodium ascorbate, 2 mM $CuSO_4$, 10 μM biotin-azide in PBS) for 1 hour. Cells were re-suspended with lysis buffer (1% SDS in 50 mM Tris-HCl pH 8.0) containing protease inhibitor cocktail (2 tablets for 10 ml). Sonication was done by the following settings: pulse 20 s pulse, 40 s pause, amplitude 25%, repeat 10 times (QSONICA Sonicator, ultrasonic processor). After the centrifuge, the supernatant was diluted with PBS by 1:1. Five %/volume of each sample was saved as input. The left of the supernatant was incubated with streptavidin-magnet beads for 1 hour, and the beads with captured DNA and proteins was washed with lysis buffer followed by 1M NaCl and another lysis buffer twice. Finally, the beads were incubated with SDS Laemmli sample buffer containing 0.2M DTT at 98°C for 25 min. The input and captured proteins were analyzed by Western blotting.

Bioinformatics analysis—ATAC and nascent strands sequences were obtained by Illumina sequencing and aligned to the genome in the form of BAM flies as described (Martin et al., 2011). Sequences were converted to BED file format using the Genomatix genome analyzer suite. The BED formatted sequences were compared to BED formatted sequence of genomic DNA. For peak finding, SICER algorithm was used with the following parameters: Window size 200 bp, Fragment size 150 bp, Gap size 600 bp, and FDR 0.01. MACS2 broad peak algorithm was also used for peak findings and quantification of signal value with the following parameters: q-value 0.01, Bandwidth 300, mfold 5–50 and Redundancy/duplicate threshold ‘auto’. Colocation analysis for Nascent strand DNA-seq and ATAC-seq was done with Coloweb software by loading their BED files.

QUANTIFICATION AND STATISTICAL ANALYSIS

Statistical analyses were carried out using GraphPad prism 7 software. Test methods are described in each figure legend. $p<0.001$ is considered significant.

Supplementary Material

Refer to Web version on PubMed Central for supplementary material.

Acknowledgments

We are grateful to Drs. Susan Garfield, Poonam Mannan, Langston Lim (Confocal Microscopy Core Facility, CCR, NCI, NIH) for providing a productive environment for confocal microscopy analyses, Dr. Arnab Ray Chaudhuri (NCI/NIH) for advising on DNA fiber assay, Drs. Cyril Ribeyre and Angelos Constantinou (University of Montpellier, France) for advising on iPOND, Drs. Shunichi Takeda and Hiroyuki Sasanuma (Department of Radiation of Genetics, Kyoto University, Japan), Dr. Kouji Hirota (Tokyo Metropolitan University, Japan) for giving us professional advices, Mr. Hiroki Kawahara, Mr. Naotoshi Hatsuta, Ms. Haruna Fujiike, Mr. Daichi Imamura (Faculty of Medicine and Graduate school of Medicine, Kyoto University, Japan) for helping experiments, the CCR sequencing facility for their help in sequencing and analyzing NS-seq and ATAC-seq data, and AstraZeneca for providing AZD-6738. We also thank to Developmental Therapeutics Program (Division of Cancer Treatment and Diagnosis, NCI/NIH) for providing drugs and cell lines used in this study. This project was supported by the Intramural Program, Center for Cancer Research of the National Cancer Institute, NIH (BC006150) (to Y.P.).

References

Aladjem MI, Redon CE. Order from clutter: selective interactions at mammalian replication origins. Nat Rev Genet. 2016

Barretina J, Caponigro G, Stransky N, Venkatesan K, Margolin AA, Kim S, Wilson CJ, Lehar J, Kryukov GV, Sonkin D, et al. The Cancer Cell Line Encyclopedia enables predictive modelling of anticancer drug sensitivity. Nature. 2012; 483:603–607. [PubMed: 22460905]

Branzei D, Foiani M. Regulation of DNA repair throughout the cell cycle. Nature reviews Molecular cell biology. 2008; 9:297–308. [PubMed: 18285803]

Buenrostro JD, Giresi PG, Zaba LC, Chang HY, Greenleaf WJ. Transposition of native chromatin for fast and sensitive epigenomic profiling of open chromatin, DNA-binding proteins and nucleosome position. Nat Methods. 2013; 10:1213–1218. [PubMed: 24097267]

Feijoo C, Hall-Jackson C, Wu R, Jenkins D, Leitch J, Gilbert DM, Smythe C. Activation of mammalian Chk1 during DNA replication arrest: a role for Chk1 in the intra-S phase checkpoint monitoring replication origin firing. J Cell Biol. 2001; 154:913–923. [PubMed: 11535615]

Fragkos M, Ganier O, Coulombe P, Mechali M. DNA replication origin activation in space and time. Nat Rev Mol Cell Biol. 2015; 16:360–374. [PubMed: 25999062]

Fu H, Besnard E, Desprat R, Ryan M, Kahli M, Lemaitre JM, Aladjem MI. Mapping replication origin sequences in eukaryotic chromosomes. Curr Protoc Cell Biol. 2014; 65:22–20. 21–17.

Gardner EE, Lok BH, Schneeberger VE, Desmeules P, Miles LA, Arnold PK, Ni A, Khodos I, de Stanchina E, Nguyen T, et al. Chemosensitive Relapse in Small Cell Lung Cancer Proceeds through an EZH2-SLFN11 Axis. Cancer Cell. 2017; 31:286–299. [PubMed: 28196596]

Josse R, Martin SE, Guha R, Ormanoglu P, Pfister TD, Reaper PM, Barnes CS, Jones J, Charlton PA, Pollard JR, et al. The ATR inhibitors VE-821 and VX-970 sensitize cancer cells to topoisomerase I inhibitors by disabling DNA replication initiation and fork elongation responses. Cancer Res. 2014; 74:6968–6979. [PubMed: 25269479]

King C, Diaz HB, McNeely S, Barnard D, Dempsey J, Blosser W, Beckmann R, Barda D, Marshall MS. LY2606368 Causes Replication Catastrophe and Antitumor Effects through CHK1-Dependent Mechanisms. Mol Cancer Ther. 2015; 14:2004–2013. [PubMed: 26141948]

Liaw H, Lee D, Myung K. DNA-PK-dependent RPA2 hyperphosphorylation facilitates DNA repair and suppresses sister chromatid exchange. PLoS One. 2011; 6:e21424. [PubMed: 21731742]

Lok BH, Gardner EE, Schneeberger VE, Ni A, Desmeules P, Rekhtman N, de Stanchina E, Teicher BA, Riaz N, Powell SN, et al. PARP Inhibitor Activity Correlates with SLFN11 Expression and Demonstrates Synergy with Temozolomide in Small Cell Lung Cancer. Clin Cancer Res. 2017; 23:523–535. [PubMed: 27440269]

Marechal A, Li JM, Ji XY, Wu CS, Yazinski SA, Nguyen HD, Liu S, Jimenez AE, Jin J, Zou L. PRP19 transforms into a sensor of RPA-ssDNA after DNA damage and drives ATR activation via a ubiquitin-mediated circuitry. Mol Cell. 2014; 53:235–246. [PubMed: 24332808]

Martin MM, Ryan M, Kim R, Zakas AL, Fu H, Lin CM, Reinhold WC, Davis SR, Bilke S, Liu H, et al. Genome-wide depletion of replication initiation events in highly transcribed regions. Genome Res. 2011; 21:1822–1832. [PubMed: 21813623]

Mavrommatis E, Fish EN, Platanias LC. The schlafen family of proteins and their regulation by interferons. Journal of interferon & cytokine research: the official journal of the International Society for Interferon and Cytokine Research. 2013; 33:206–210.

Mu Y, Lou J, Srivastava M, Zhao B, Feng XH, Liu T, Chen J, Huang J. SLFN11 inhibits checkpoint maintenance and homologous recombination repair. EMBO Rep. 2016; 17:94–109. [PubMed: 26658330]

Murai J, Feng Y, Yu GK, Ru Y, Tang SW, Shen Y, Pommier Y. Resistance to PARP inhibitors by SLFN11 inactivation can be overcome by ATR inhibition. Oncotarget. 2016; 7:76534–76550. [PubMed: 27708213]

Murai J, Huang SY, Das BB, Renaud A, Zhang Y, Doroshow JH, Ji J, Takeda S, Pommier Y. Trapping of PARP1 and PARP2 by Clinical PARP Inhibitors. Cancer Res. 2012; 72:5588–5599. [PubMed: 23118055]

Nogales V, Reinhold WC, Varma S, Martinez-Cardus A, Moutinho C, Moran S, Heyn H, Sebio A, Barnadas A, Pommier Y, et al. Epigenetic inactivation of the putative DNA/RNA helicase SLFN11 in human cancer confers resistance to platinum drugs. Oncotarget. 2016; 7:3084–3097. [PubMed: 26625211]

Petermann E, Woodcock M, Helleday T. Chk1 promotes replication fork progression by controlling replication initiation. Proceedings of the National Academy of Sciences of the United States of America. 2010; 107:16090–16095. [PubMed: 20805465]

Pommier Y. Topoisomerase I inhibitors: camptothecins and beyond. Nat Rev Cancer. 2006; 6:789–802. [PubMed: 16990856]

Ray Chaudhuri A, Hashimoto Y, Herrador R, Neelsen KJ, Fachinetti D, Bermejo R, Cocito A, Costanzo V, Lopes M. Topoisomerase I poisoning results in PARP-mediated replication fork reversal. Nat Struct Mol Biol. 2012; 19:417–423. [PubMed: 22388737]

Ribeyre C, Zellweger R, Chauvin M, Bec N, Larroque C, Lopes M, Constantinou A. Nascent DNA Proteomics Reveals a Chromatin Remodeler Required for Topoisomerase I Loading at Replication Forks. Cell Rep. 2016; 15:300–309. [PubMed: 27050524]

Seiler JA, Conti C, Syed A, Aladjem MI, Pommier Y. The Intra-S-Phase Checkpoint Affects both DNA Replication Initiation and Elongation: Single-Cell and -DNA Fiber Analyses. Mol Cell Biol. 2007; 27:5806–5818. [PubMed: 17515603]

Sirbu BM, Couch FB, Cortez D. Monitoring the spatiotemporal dynamics of proteins at replication forks and in assembled chromatin using isolation of proteins on nascent DNA. Nat Protoc. 2012; 7:594–605. [PubMed: 22383038]

Stewart CA, Tong P, Cardnell RJ, Sen T, Li L, Gay CM, Masrorpour F, Fan Y, Bara RO, Feng Y, et al. Dynamic variations in epithelial-to-mesenchymal transition (EMT), ATM, and SLFN11 govern response to PARP inhibitors and cisplatin in small cell lung cancer. Oncotarget. 2017

Syljuasen RG, Sorensen CS, Hansen LT, Fugger K, Lundin C, Johansson F, Helleday T, Sehested M, Lukas J, Bartek J. Inhibition of human Chk1 causes increased initiation of DNA replication, phosphorylation of ATR targets, and DNA breakage. Mol Cell Biol. 2005; 25:3553–3562. [PubMed: 15831461]

Toledo LI, Altmeyer M, Rask MB, Lukas C, Larsen DH, Povlsen LK, Bekker-Jensen S, Mailand N, Bartek J, Lukas J. ATR prohibits replication catastrophe by preventing global exhaustion of RPA. Cell. 2013; 155:1088–1103. [PubMed: 24267891]

Weibezahn J, Schlieker C, Bukau B, Mogk A. Characterization of a trap mutant of the AAA+ chaperone ClpB. The Journal of biological chemistry. 2003; 278:32608–32617. [PubMed: 12805357]

Yang W, Soares J, Greninger P, Edelman EJ, Lightfoot H, Forbes S, Bindal N, Beare D, Smith JA, Thompson IR, et al. Genomics of Drug Sensitivity in Cancer (GDSC): a resource for therapeutic biomarker discovery in cancer cells. Nucleic Acids Res. 2013; 41:D955–961. [PubMed: 23180760]

Zeman MK, Cimprich KA. Causes and consequences of replication stress. Nat Cell Biol. 2014; 16:2–9. [PubMed: 24366029]

Zhang YW, Brognard J, Coughlin C, You Z, Dolled-Filhart M, Aslanian A, Manning G, Abraham RT, Hunter T. The F box protein Fbx6 regulates Chk1 stability and cellular sensitivity to replication stress. Mol Cell. 2009; 35:442–453. [PubMed: 19716789]

Zoppoli G, Regairaz M, Leo E, Reinhold WC, Varma S, Ballestrero A, Doroshow JH, Pommier Y. Putative DNA/RNA helicase Schlafen-11 (SLFN11) sensitizes cancer cells to DNA-damaging agents. Proc Natl Acad Sci U S A. 2012; 109:15030–15035. [PubMed: 22927417]

HIGHLIGHTS

- SLFN11 binds replication forks in response to replication stress
- SLFN11 blocks replication regardless of ATR-CHK1 activity
- SLFN11 opens chromatin in the near vicinity of replication initiation sites
- By killing cells with defective replication, SLFN11 arises a guardian of the genome

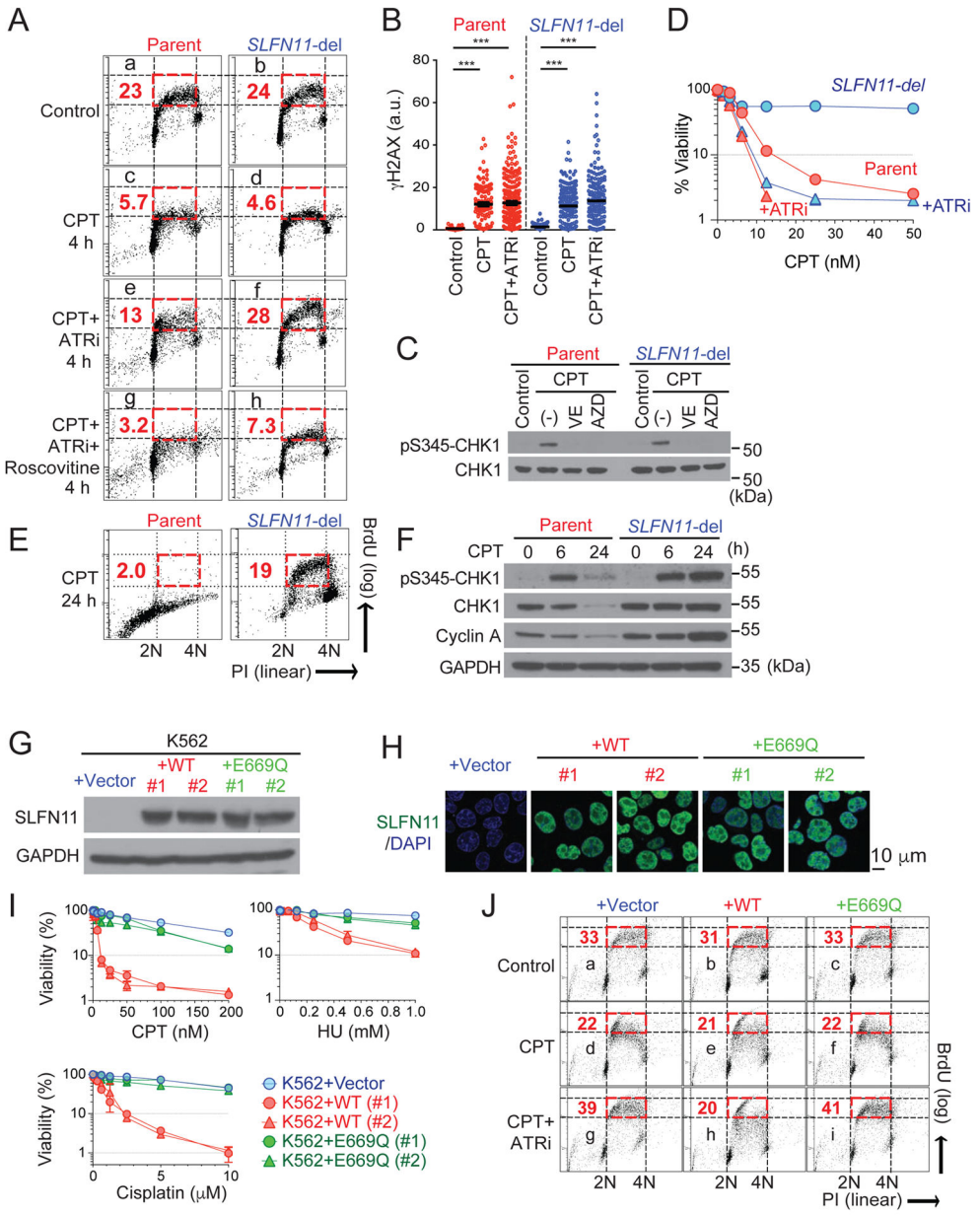

Figure 1. SLFN11 requires its ATPase activity to block replication independently of ATR and does not affect γ H2AX and ATR activation

(A–F) Functional analyses of SLFN11 in CCRF-CEM parental and *SLFN11*-del cells. (A) Representative flow cytometry cell cycle data in response to CPT (100 nM), ATRi (AZD6738 or VE-821; 1 μM) and roscovitine (20 μM). The percentage of highly replicating cells is annotated (red dashed boxes and numbers; average of 3 independent experiments). PI: propidium iodide. (B) γH2AX measured by immunofluorescence 4 hours after drug treatment [100 nM CPT, 1 μM ATRi (VE-821)]. Error bars represent mean ± standard error of the mean (SEM, n = 113–238). ***p ≤ 0.0001 (two-tailed unpaired t test). (C) Western blot for phospho-S345 CHK1 and total CHK1. VE: VE-821, AZD: AZD6738. (D) Viability curves for CPT alone (circles) and with ATRi (triangles) (mean ± SD, n = 3). Data are

representative of three independent experiments. (E) Representative flow cytometry cell cycle data after 24 hour CPT (100 nM) treatments. (F) Representative Western blot for CHK1 activation and degradation, and cyclin A levels using whole cell extracts.
(G–H) SLFN11 expression in the indicated K562 cell lines measured by Western blotting (G) and immunofluorescence without pre-extraction (H).
(I) Drug resistance of the ATPase-defective SLFN11 cells (mean ± SD, n = 3). Data are representative of two independent experiments.
(J) Representative cell cycle analyses after 4 hours treatments [250 nM CPT, 1 μM ATRi (VE-821)] shown as (A).
(See also Figure S1)

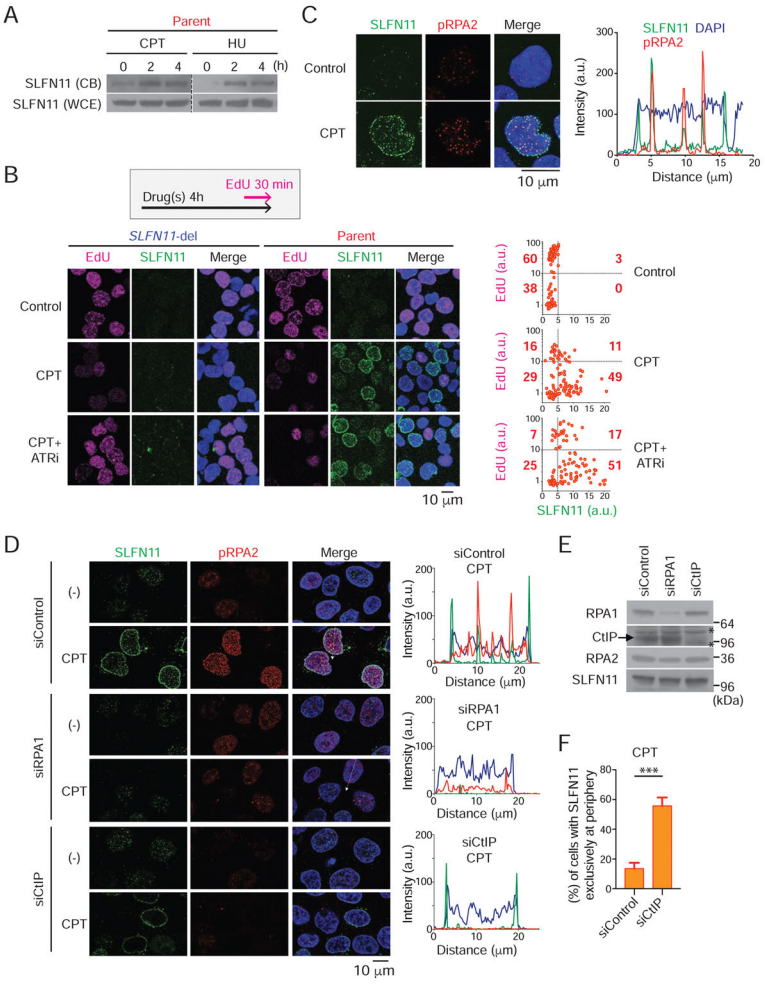

Figure 2. SLFN11 is recruited to chromatin and the nuclear periphery via RPA1, where it blocks replication in response to replication stress

(A) Western blots of chromatin bound fraction (CB) and whole cell extract (WCE) in CCRF-CEM parental cells [100 nM CPT, 0.5 mM HU].

(B–C) Immunofluorescence analyses in CCRF-CEM *SLFN11*-del and parental cells treated as indicated [100 nM CPT, 1 μM ATRi (AZD6738)] for 4 h. (B left) Drug treatment and replication labelling scheme and representative confocal microscopy images; DNA replication foci (EdU, purple), chromatin bound SLFN11 (green) and DAPI (blue). (B right) Correlations between EdU and SLFN11 signals in individual cells for the indicated treatments. Thresholds for EdU (10) and SLFN11 (5) were set from distributions in the control experiment. The percentage of cells in each segment is annotated as bold red numbers (n = 108–110). Results are representative of two independent experiments. **(C)** Representative images of chromatin-bound SLFN11 (green), phospho-RPA2 (S4/S8) (red) and DAPI (blue) (left), and tracing of the distribution of signals along the white dashed arrow shown in the merged panel (right).

(D) Representative confocal microscopy images for chromatin bound SLFN11 (green), phospho-RPA2 (S4/S8) (red) and DAPI (blue) in DU145 parental cells. Representative

tracings are shown at right. Cells were transfected with control siRNA (siControl) or siRNA for RPA1 or CtIP (siRPA1; siCtIP) for 48 hours before 4 hour CPT treatments (100 nM). **(E)** Efficiency of the siRNAs determined by Western blot with whole cell extract. **(F)** Percentage of cells having SLFN11 signals exclusively at the nuclear periphery after CPT treatment in siControl and siCtIP treated cells (mean ± SD; n = 4; 60–117 cells with SLFN11 signal at nuclear periphery were examined in each sample). ***$p \leq 0.0001$ (two-tailed unpaired t test).
(See also Figure S2)

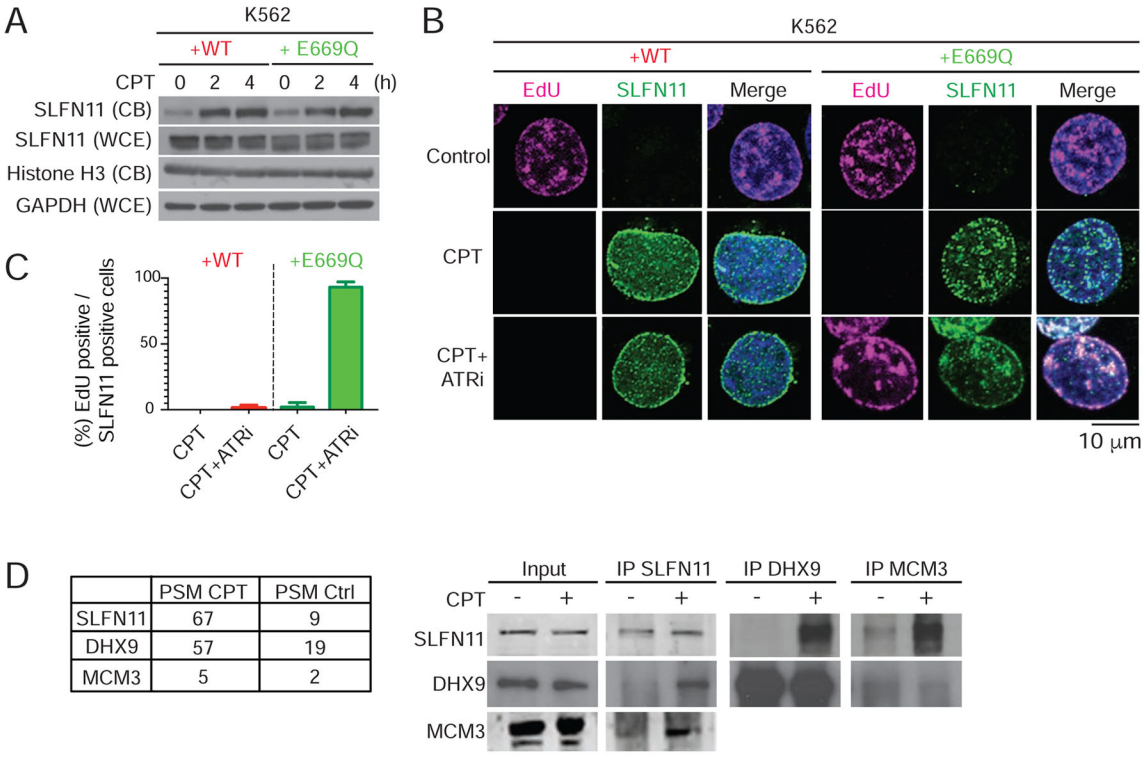

	PSM CPT	PSM Ctrl
SLFN11	67	9
DHX9	57	19
MCM3	5	2

Figure 3. SLFN11 localizes to replication foci and binds MCM3 and DHX9 in response to CPT and the ATPase domain of SLFN11 is required to block replication but not for chromatin recruitment

(A) SLFN11 binds chromatin independently of its ATPase domain. Western blots of chromatin bound fraction (CB) and whole cell extract (WCE) (CPT 250 nM). Histone H3 and GAPDH were used as control.

(B–C) Immunofluorescence of DNA replication foci (EdU) (purple) and chromatin-bound SLFN11 (green). Treatments were for 4 hours [250 nM CPT and 1 μM ATR inhibitor (ATRi) AZD6738]. EdU was added 30 min before cell collection. (B) Representative confocal microscopy images. (C) Percentage of EdU-positive cells in the *SLFN11*-positive cells (mean ± SD, n = 3; >30 SLFN11-positive cells were examined in each sample).

(D) Binding of SLFN11 to MCM3 and DHX9. Immunoprecipitation with anti-SLFN11 antibody (E-4) was coupled with mass spectrometry (IP-MS) using nuclear fractions of DU145 parental cells (left). Confirmation of the IP-MS results using antibodies against SLFN11 (E-4), DHX9 and MCM3 (right). Ctrl: control, PMS: peptide spectrum match. Whole data are listed in Table S1 (control) and S2 (CPT-treated).

(See also Figure S3, Table S1 and S2)

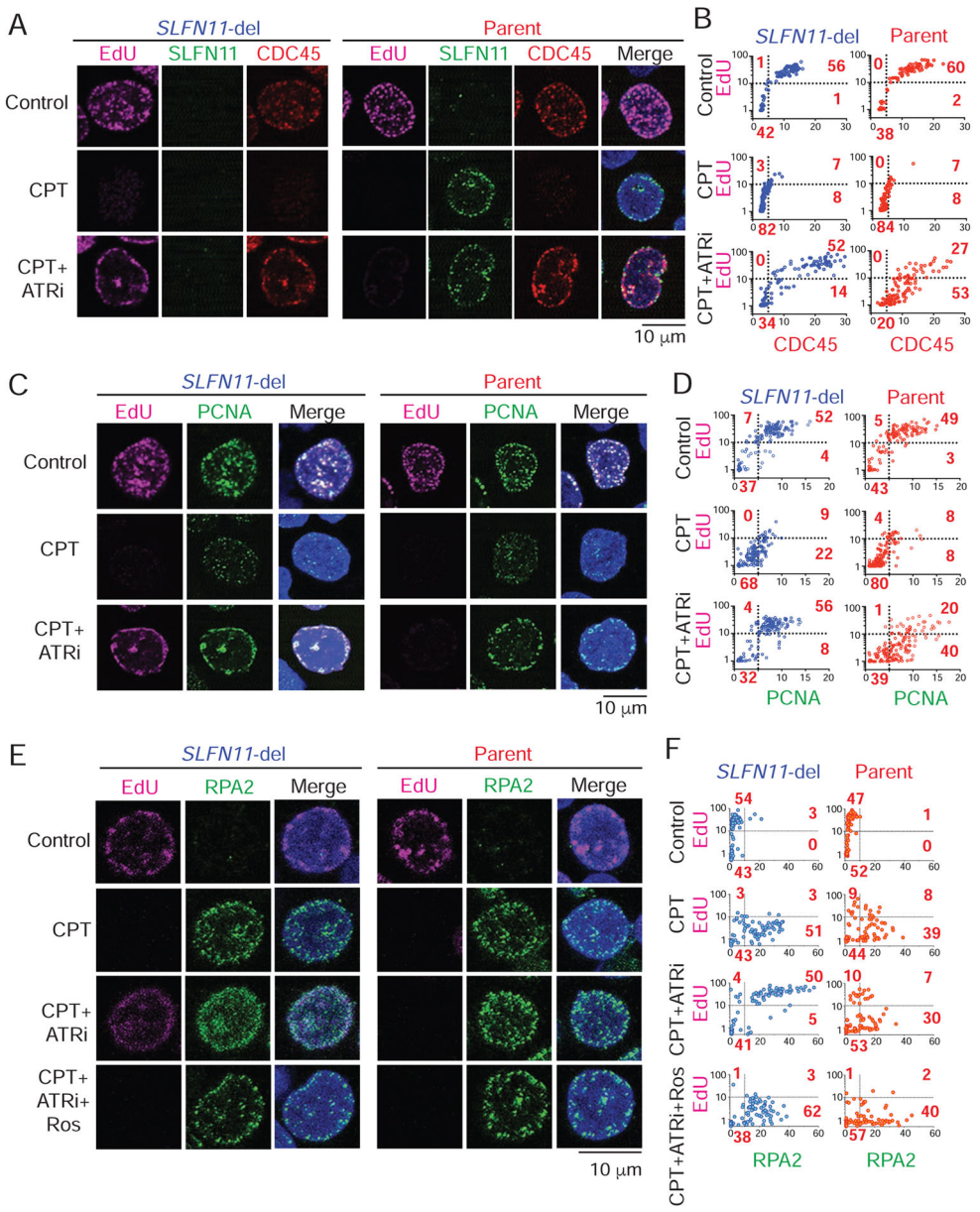

Figure 4. SLFN11 binding to chromatin does not interfere with CDC45 and PCNA loading but blocks RPA extension and replication in response to CPT

(A, C and E) Representative confocal microscopy images for replication foci (EdU), CDC45 and SLFN11 (A), PCNA and EdU (C), and RPA2 and EdU (E)]. CCRF-CEM *SLFN11*-del and parental cells were treated for 4 hours [100 nM CPT, 1 μM ATR inhibitor (ATRi) (AZD6738) and 20 μM roscovitine (Ros)].

(B, D and F) Quantification of A, C, and D, respectively, and correlations between EdU and the indicated chromatin-bound proteins. Data are shown as Figure 2B. n = 104–113 (B), n = 150–158 (D), n = 101–102 (F). Data are representative of two independent experiments. (See also Figures S4 and S5)

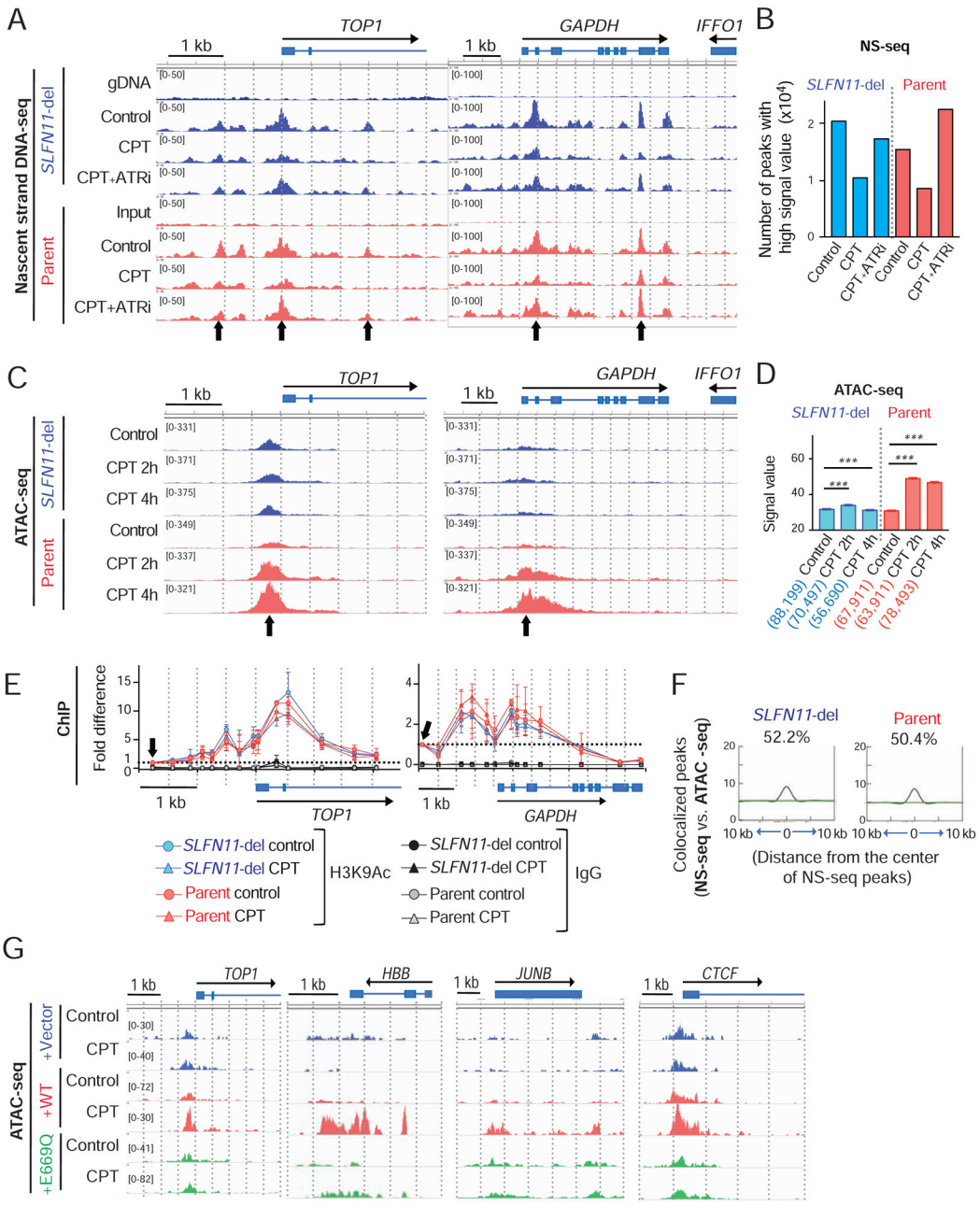

Figure 5. SLFN11 does not interfere with the initiation of DNA replication but opens chromatin in the vicinity of the initiation sites in response to CPT

(A) Sequencing tracks of nascent strand DNA-seq for the *TOP1* and *GAPDH* loci in CCRF-CEM *SLFN11*-del (blue) and parental cells (red). Drug treatments were for 4 hours [100 nM CPT, 2 μM ATRi (VE-821)]. Arrows indicate center of peaks. gDNA: genomic DNA.

(B) Bar graphs summarizing the number of high intensity replication initiation peaks determined by NS-seq. Calculations used MACS2 broad peak analysis and peaks with signal value >50 are plotted.

(C) Representative sequencing tracks of ATAC-seq for the *TOP1* and *GAPDH* loci in CCRF-CEM *SLFN11*-del (blue) and parental cells (red). Cells were treated with 100 nM

CPT. Each height is adjusted by total read number after trimming in each sample (Table S3). Arrows indicate center of peaks.

(D) Bar graphs representing signal values for all peaks of each ATAC-seq data calculated using MACS2 broad peak analysis (mean ± SEM). The number of peak in each condition is shown in parentheses. ***$p \leq 0.0001$ (two-tailed unpaired t test).

(E) Enrichment of the active histone mark H3K9Ac at *TOP1* and *GAPDH* loci is similar in CCRF-CEM *SLFN11*-del (blue) and parental (red) cells with or without CPT treatment (100 nM, 4h) analyzed by chromatin immunoprecipitation (ChIP) assay. Values (bound/input, mean ± SD, n = 3–4) represent fold enrichments normalized to background level for anti-H3K9Ac antibody (arrow in each panel).

(F) Co-localization between NS-seq peaks as regions of interest (ROI) and ATAC-seq peak regions as features in CCRF-CEM *SLFN11*-del (left) and parental cells (right) using the Coloweb co-localization analysis tool. Peak data were obtained using the SICER algorithm. Windows were centered on peaks from NS-seq (ROI). The percentage of ROI collocated with the feature are shown above in each panel. A ROI is counted as co-located if it has at least one feature within the window size (20 kb).

(G) Sequencing tracks of ATAC-seq for representative initiation loci (*TOP1, HBB*, *JUNB* and *CTCF*) in K562 cells. The indicated cells were treated as indicated (CPT 1 μM) for 4 hours. Each height is adjusted by total read number after trimming of each sample (Table S3).

(See also Figures S6)

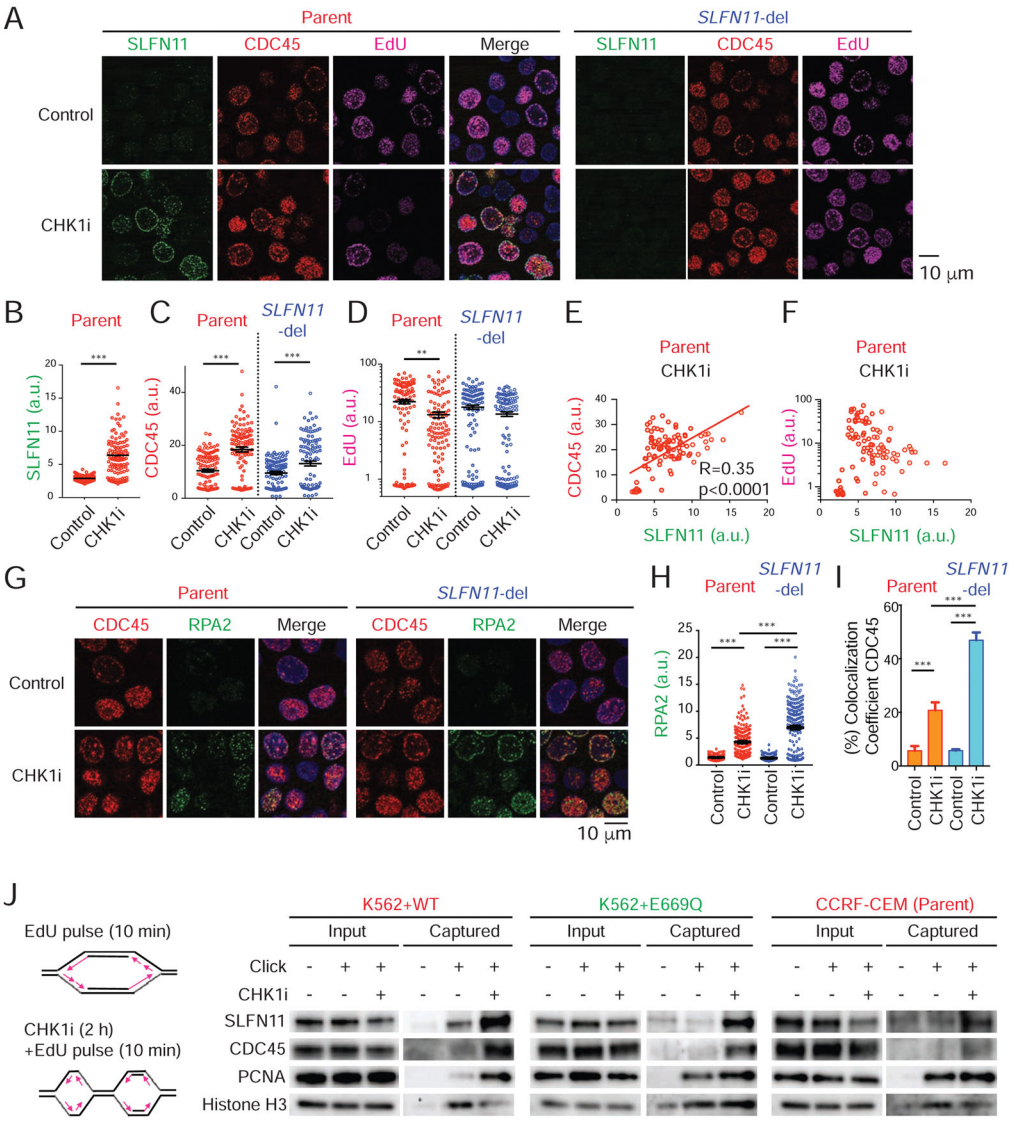

Figure 6. SLFN11 binds stressed replication forks in response to CHK1 inhibition and blocks replication and RPA extension

(A–F) Immunofluorescence analysis for DNA replication (EdU) (purple), chromatin-bound SLFN11 (green), CDC45 (red) and DAPI (blue). CCRF-CEM parental and *SLFN11*-del cells were treated for 4 hours with CHK1 inhibitor (CHK1i, LY2606368, 10 nM]. EdU was added 30 min before cell collection. **(A)** Representative confocal microscopy images. **(B–D)** Distribution of mean signal intensity of individual nuclei for SLFN11 (B), CDC45 (C), and EdU (D). Mean ± SEM. **(E)** Correlation between CDC45 and SLFN11 signals (R: Pearson correlation coefficient; red line: linear regression curve). **(F)** Relationship between EdU and SLFN11 signals [n = 109–114 (B–F)]. Data are representative of two independent experiments. ***p ≤ 0.0001, **p ≤ 0.001 (two-tailed unpaired t test).

(G–I) Immunofluorescence analyses for chromatin bound RPA2 (green), CDC45 (red) and DAPI (blue). CCRF-CEM parental and *SLFN11*-del cells were treated as in panels (A–F). **(G)** Representative confocal microscopy images. **(H)** Distribution of mean signal intensity

of individual nuclei for RPA2 (mean ± SEM; n = 116–202). **(I)** Co-localization of CDC45 with RPA2. Calculations were derived from 5–7 images (130 μm × 130 μm) containing ~50 cells/image (mean ± SD). ***p ≤ 0.0001 (two-tailed unpaired t test).
(J) Western blot analysis with the indicated antibodies for input and captured proteins isolated by iPOND. The indicated cells were treated with CHK1i (100 nM) for 2 hours, and pulse-labeled with EdU for 10 min just before collecting cells (scheme on the left).
(See also Figures S7)

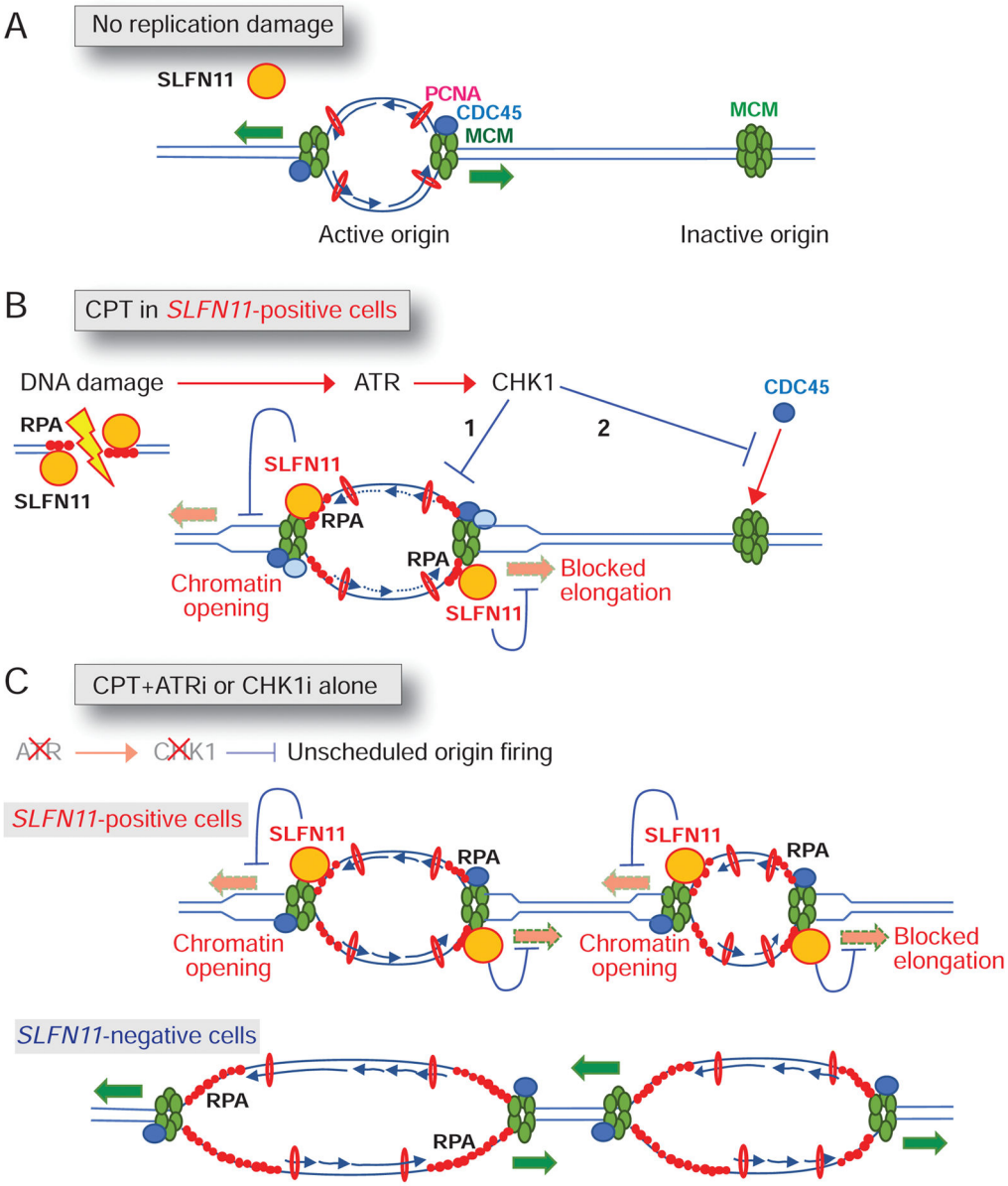

Figure 7. Molecular model of SLFN11-induced replication fork block in response to replication stress

(A) Replication without replicative stress. **(B)** Replication stress induced by CPT in *SLFN11*-positive cells. **(C)** Unscheduled origin firing induced by CPT+ATR inhibitor or by CHK1 inhibitor in *SLFN11*-positive (top) and *SLFN11*-negative cells (bottom) (see Discussion for details).